# Viscoelastic *damping*| in high rise structures

A feasibility study on the development of a **prototype tool** for engineering firms which can be used to determine the required amount of **viscoelastic damping** in a **high rise structure** to reduce **accelerations** from **wind-induced vibrations** to a comfortable level

Main report



D.A.J. Hilster







#### **COLOPHON**

TITLE Viscoelastic damping in high rise structures

SUBTITLE A feasibility study on the development of a prototype tool

to determine the required amount of viscoelastic damping in a high rise structure to reduce accelerations from wind-

induced vibrations

DATE October 2013

AUTHOR D.A.J. (Denise) Hilster

Pre-education: TU Delft BSc Industrial Design

Bridging program Civil Engineering

Current education: TU Delft MSc Civil Engineering

Track: Building Engineering Specialization: Structural Design

CONTACT AUTHOR Pletterijkade 19D

2515 SG Den Haag Mobile: 06 19 96 11 08

E-mail: denisehilster@gmail.com

**GRADUATION** prof. ir. R. Nijsse (chair)

**COMMITTEE** (Department Building Engineering)

TU DELFT prof. dr. A.V. Metrikine

(Department Structural Mechanics)

ir. S. Pasterkamp

(Department Building Engineering)

**CONTACT** ir. A. Robbemont

ZONNEVELD Zonneveld Ingenieurs by INGENIEURS Delftseplein 27 (floor 8)

3013 AA Rotterdam (010) 452 88 88

CONTACT dr. ir. R.D.J.M. Steenbergen

TNO BOUW prof. ir. A.C.W.M Vrouwenvelder & ONDERGROND van Mourik Broekmanweg 6

2628 XE Delft (088) 866 30 00

# Viscoelastic damping in high rise structures

A feasibility study on the development of a prototype tool to determine the required amount of viscoelastic damping in a high rise structure to reduce accelerations from wind-induced vibrations

MAIN REPORT

 $01\mathrm{em}$ 

### **Preface**

This thesis is the result of a graduation project in the master program 'Building Engineering' at Delft University of Technology. The research has been conducted in cooperation with the companies Zonneveld Ingenieurs and TNO Bouw & Infra. The project is a feasibility study on the development of a prototype tool to determine the required amount of viscoelastic damping in a high rise structure to reduce accelerations from wind-induced vibrations. Tests have been conducted in the lab with a portal frame structure including a self-designed damping component and theoretical models have been developed to describe commonly used structural systems in high rise structures.

First of all I would like to thank my TU Delft supervisors prof. ir. R. Nijsse, ir. S. Pasterkamp and prof. dr. ir. A. Metrikine for their time and feedback during the project. Especially ir. S. Pasterkamp, who has always been available on short notice to answer my questions and listen to the struggles I had.

Next, I would like to thank my supervisors from TNO, dr. ir. R.D.J.M. Steenbergen who took a lot of time and effort to read my work and prof. ir. A.C.W.M. Vrouwenvelder. Their expertise and constructive criticism has challenged me to increase the level of my work. Special thanks goes out to ir. L. Vredeveldt for his guidance throughout the process of setting up my experiment, conducting the tests and the data analysis. His knowledge and positive attitude has really encouraged me throughout the process. Also, I would like to the thank the guys from the TNO lab for their help with the structure of my experiment.

Then, I would like to thank ir. A. Robbemont, my supervisor from Zonneveld Ingenieurs, who has helped me to keep a practical approach to my work and who always had confidence in the subject of my thesis and me. Also, I'd like to thank my colleagues at Zonneveld Ingenieurs for the pleasant working environment and being open to my questions at all times.

Thanks goes out to Vilton for providing me the SBR layers for the experiments.

Also, thanks to Maarten for being a sound board whenever I needed it. Also to my beloved parents, brother and Radna who have always had faith in my capabilities. Your words have always motivated me to get the best out of myself.

Thanks goes out to Daan, Sander and Janne, who were always open for discussions regarding my work and graduation process. Also to Paul, who helped me to improve my Matlab skills. To Nadine and Frank, who were in the same boat as we worked through the summer together and thanks to all my other friends I have not mentioned here by name for supporting me and for willing or unwillingly listening to me.

Denise Hilster Den Haag, October 2013

# Summary

#### Introduction

The research regarding damping in high rise structures from wind-induced vibrations has been split up into two investigations:

- 1. Investigation on viscoelastic damping (VED)
- 2. Investigation on modeling a N mass spring damper (N-MSD) system as a basis for the prototype tool

Literature showed that VEDs are most effective in shear and even though a VED is often referred to as non-linear, the material behaves linear for small values of the damping ratio. This region has been studied in the investigation on VED.

#### Physical test set-up

In literature, no information is available on the relation of VEDs to the load bearing structure in buildings. Therefore, a physical test set-up was built to study the relation. The physical test set-up was constructed as a braced portal frame structure with a slenderness of about 6. Layers of SBR (natural rubber) were applied to the bracing to simulate dampers in a structure. Multiple dampers have been tested with a variety in thickness. This was based on the expectation that the thickness of the layers would have an optimum value with regards to the shear stiffness. The half-power bandwidth method was used to determine the damping ratio of the structure with and without damping in the frequency domain. To verify the obtained values, the damping ratio has also been determined from the time signal through the logarithmic decrement. Both methods showed the same results.

#### N-MSD

In this research, a model has been presented for the core structure with structural damping by means of an N-MSD system. The model has been validated in two ways. The stiffness matrix was validated by finding the static behavior of the structure and the eigenmodes from the structure. Additionally, the peak values for the accelerations come close to the maximum allowed values mentioned in NEN-EN 1990+A1+A1/C2-2011. Also, a mathematical set-up for a braced portal frame structure including an auxiliary damping component has been presented. In this case, all elements in the portal frame structure are described by a continuous system. Additionally, a model for the bracing with and without a damping component is to be used.

#### Conclusions

The following damping factors were observed within the damping component:

- 1. Damping by friction
- 2. Material damping
- 3. Damping by adhesive layer (glue)

If a higher damping coefficient is required to reduce accelerations, each of these factors may be changed. However, the exact energy dissipation by each individual factor in the damping component and in the connections remains still unknown. The only certainty is that the system as a whole dissipates energy from the structural system and reduces the accelerations. The measurements were also influenced by many factors, such as disturbances from higher frequencies and executional factors.

The description of the core structure model and of the portal frame structure prove that it is vi SUMMARY

determine the required amount of VED. However, in case a prototype tool is to be developed,

indeed feasible to develop a prototype tool to input of experimental data of the damping coefficient of the VEM layer is required.

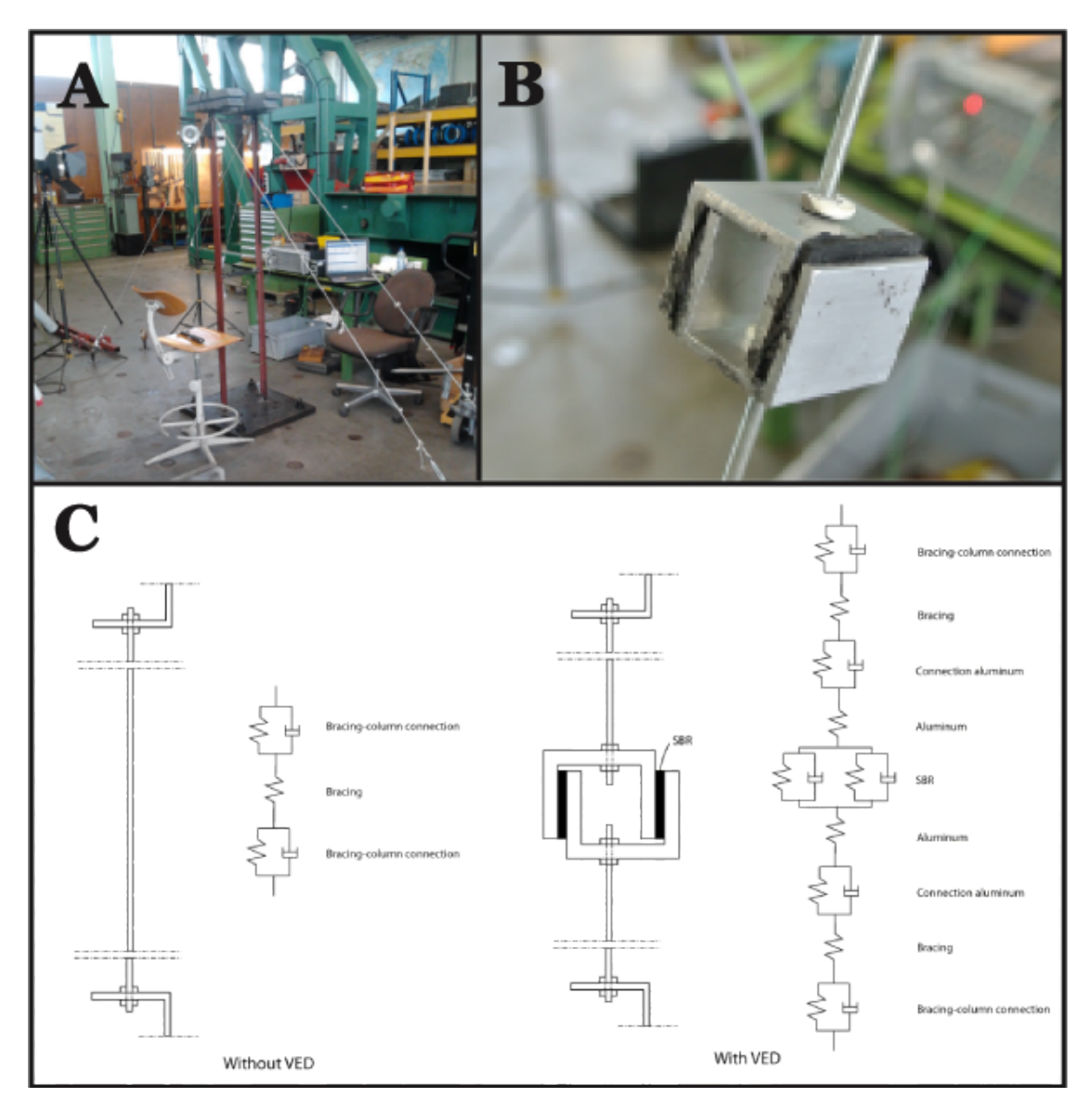


Figure 1: Physical test set-up and N-MSD model

# Contents

P	reface	iv
Sı	ımmary	v
Li	st of symbols and abbrevations	viii
$\mathbf{G}$	lossary of terms	xii
1	Introduction 1.1 Relevance of this thesis	<b>2</b> 2
	1.2 How to read this report?	
2	Results of literature review 2.1 High rise structures	<b>6</b>
	2.2       Dynamic wind load	7 9
3	2.4 Damping	10 <b>15</b>
J	3.1 General description of investigations	15 16 23
4	Vibrations in high rise structures 4.1 Model set-up	33 38 38 44 50
5	Conclusions5.1 Conclusions5.2 Extrapolation of the results5.3 Recommendations	<b>52</b> 52 57 58
6	Summary of conclusions	61

# List of symbols and abbrevations

#### Latin symbols, capitals

$A_i$	surface area	$[\mathrm{m}^2]$
B	structural factor	[-]
$C_p$	stagnation pressure coefficient	[-]
$C_y$	decay factor of the coherence y-direction (width)	[-]
$C_y \\ C_z$	decay factor of the coherence direction (height)	[-]
E'	storage modulus longitudinal	$[N/m^2]$
E''	loss modulus shear longitudinal	$[N/m^2]$
$E^*$	dynamic modulus shear longitudinal	$[N/m^2]$
E	energy	[Nm]
	Young's modulus	$[N/m^2]$
E	time dependent Young's modulus	$[N/m^2]$
EI	flexural rigidity	$[N/m^2]$
F	force	[N]
$F_0$	force	[N]
$F_c$	Coriolis force	[N]
$F_D$	Solari's spectrum of wind load	[-]
$F_w$	wind load	[N]
G'	storage modulus shear	$[N/m^2]$
G''	loss modulus shear	$[N/m^2]$
$G^*$	dynamic modulus shear	$[N/m^2]$
G	shear modulus	$[N/m^2]$
H	frequency response function	[differs]
$I_v$	turbulence intensity	[-]
J	rotational moment of inertia	$[m^4/rad]$
$K_x$	dimensionless coefficient	[-]
L	length	[m]
	scale of turbulence	[m]
M	moment	[Nm]
N	number of frequency intervals	[-]
R	resonance response factor	[-]
Re	Reynolds number	[-]
	real number	[-]
T	period	[s]

$S_{aa}$	spectrum of accelerations	$[m^2/s^2]$
$S_L$	dimensionless spectral density function	[-]
$S_{uu}$	spectrum of displacements	$[\mathrm{m}^2]$
$S_{vv}$	spectrum of wind gusts	$[\mathrm{m}^2/s]$
V	volume	$[\mathrm{m}^3]$
X	amplitude	[-]

#### Latin symbols, regular

a	acceleration	$[\mathrm{m/s^2}]$
b	width of the building	[m]
$c^*$	modal damping coefficient	[Ns/m]
c	damping coefficient	[Ns/m]
$c_0$	orographic factor	[-]
$c_f$	force coefficient	[-]
$c_r$	roughness factor	[-]
$coh_{vv}$	coherence of the wind speeds	[-]
d	zero-plane displacement	[m]
	depth of the structure	[m]
f	frequency	[Hz]
$f_L$	dimensionless frequency	[-]
g	peak factor taking into account the wind gusts	[-]
h	height of the structure	[m]
$h_r$	aspect ratio	[-]
$k^*$	modal spring stiffness	[N/m]
k	spring stiffness	[N/m]
$k_l$	turbulence factor	[-]
$k_p$	peak factor	[-]
$k_r$	terrain factor	[-]
$m^*$	modal mass	[kg]
m	mass	[kg]
$n_i$	eigenfrequency of the structure	[Hz]
$p_0$	pressure at stagnation point	$[N/m^2]$
$p_e$	pressure at point $e$	$[N/m^2]$
$q_{w,i}$	distributed wind pressure	[N/m]
s	number of frequency	[-]
t	time	[s]
u	displacement in x-direction	[m]
$\bar{v}$	mean part of the wind velocity	$[\mathrm{m/s}]$
$ ilde{v}$	variable part of the wind velocity	$[\mathrm{m/s}]$
v	velocity	$[\mathrm{m/s}]$
$v_0$	velocity at stagnation point	[m/s]
$v_b$	basic wind speed	$[\mathrm{m/s}]$
$v_e$	velocity at point e	[m/s]
$v_m$	average wind speed	[m/s]
x	parallel to wind direction	[m]
	variable	[-]
y	perpendicular to wind direction	[m]

z	height above ground level (vertical direction)	[m]
$z_0$	roughness length	[m]
$z_{min}$	minimum height	[m]
$z_G$	gradient height	[m]

#### Greek symbols, capital

$\Phi$	amplitude	[-]
$\Psi$	reduction factor	[-]
	phase shift rubber	[-]

#### Greek symbols, regular

$\alpha$	exponent	[-]
	magnification factor hysteresis loop	[-]
$\gamma$	shear strain	[-]
δ	logaritmic decrement of damping	[-]
$\varepsilon$	strain	[-]
ζ	damping ratio	[-]
$\eta$	viscosity	[kg/(sm)]
	loss factor	[-]
heta	angle	[rad]
	phase angle	[rad]
$\mu$	dynamic viscosity	$[\mathrm{Ns/m^2}]$
	friction coefficient	[-]
ho	density	$[{ m kg/m^3}]$
$\sigma$	stress	$[\mathrm{N/m^2}]$
$\sigma_f$	standard deviation of wind load	[N]
$\sigma_v$	standard deviation of wind gusts	[m/s]
au	shear stress	$[\mathrm{N/m^2}]$
$ au_0$	maximum Reynolds stress	$[\mathrm{N/m^2}]$
$\varphi$	rotation	[rad]
$\chi^2$	aerodynamic admittance	[-]
$\psi$	phase shift between stress and strain	[-]
$\omega$	angular frequency	[rad/s]
$\omega_0$	fundamental frequency	[rad/s]

#### Matrix symbols

C	domanin a montair
C	damping matrix
K	stiffness matrix
M	mass matrix
$\phi$	eigenvector matrix
$\phi^T$	transpose of eigenvector matrix

#### **Indices**

 $\begin{array}{ll} a & \text{acceleration} \\ ae & \text{aerodynamic} \\ av & \text{average} \end{array}$ 

d auxiliary damping

 $\begin{array}{ccc} diss & dissipated \\ dyn & dynamic \\ eq & equivalent \end{array}$ 

*i* number of eigenfrequency

j j th interval in spectral density function

 $egin{array}{lll} max & \max & \max & \\ min & \min & \\ s & structural & \\ stat & static & \\ tot & total & \\ \end{array}$ 

u displacement

 $egin{array}{ll} x & & \mbox{parallel to wind direction} \\ y & & \mbox{perpendicular to wind direction} \\ \end{array}$ 

z vertical direction

 $\varphi$  rotational

#### Abbreviations

FD friction damper / damping
FRF frequency response function
RK4 foruth method of Runge-Kutta
1MSD single mass-spring-damper
NMSD n mass-spring-damper

SBRx styrene-butadiene (natural rubber); x being the thickness of

the layer in mm

VD viscous damper / damping VED viscoelastic damper / damping

VEM viscoelastic material

# Glossary of terms

**Aeroelastic:** Structure where the aerodynamic, elastic and inertial forces interact

Amorphous: solid which is not fluid below its solidification temperature and which does not contain a crystalline or orderly structure

**Drag:** The drag of an object is the resistance to motion caused by air

**Gusts:** Fluctuations of wind velocity around the mean

High rise structures buildings which are affected by lateral forces due to wind or earth-quake actions to an extent that they play an important role in the structural design because of the building's height and usually contain elevators and a lot of vertical transportation of persons takes place in vertical direction

Passive damper: dampers which do not require additional energy and dissipate energy from a structural system. The response of the damper is quite slow but costs are relatively low and it will never behave as a resonance system

**Reynolds number:** The Reynolds number is defined as the ratio of fluid inertia forces (the resistance to change or motion) to viscous

forces and it is a dimensionless number. The Reynolds number is used to determine pressure coefficients and to characterize different flows, like laminar or turbulent flows. The formula to determine the Reynolds number is: [13;27]

$$Re = \frac{\rho VL}{\mu} \tag{1}$$

Reynolds stress: The Reynolds stress is defined as the net rate of transfer of momentum across a surface in a fluid resulting from turbulence in the fluid

Slip trigger displacement: the value of the displacement of a system at which it leaves its stick state

**Steady state motion:** The stable motion of a system in its equilibrium

**Vortices:** Circular, spinning motions of wind in a turbulent wind flow by a periodic release of Van Karman vortices. This release causes an alternating load perpendicular to the wind direction.

Wind: The perceptible flow of a current of air from high pressure areas to low pressure areas which arise from various causes  $01\mathrm{em}$ 

## 1 Introduction

High rise structures are an efficient way of using space since only a limited surface area at ground level is required. Also, the structure provides a large floor area in the building because of the many available floor levels. From an aesthetical point of view, architects and structural engineers want to design a building which is taller and more appealing than buildings designed by others. Of course the development of high rise structures brings along negative aspects as well. For example, fire safety regulations are much harder to meet due to the height of the building. However, past and current developments have led to better conditions in terms of fire safety so it is expected this will become less of an issue over time. [1;37]

As opposed to what the name suggests, a high rise structure is not defined by its height only. Slenderness is governing for the vibrational behavior of the structure and thus high rise structures are defined as:

**Definition 1** High rise structures are buildings which are affected by lateral forces due to wind actions with an aspect ratio of  $h/d \geq 5$ , because for these buildings the dynamic response is largest which plays an important role in the structural design of the building. [37]

Hence, the vibrational behavior must already be investigated during the design process of a building. This will become more and more important since high rise structures will be built more often in the future. Also, new regulations require better insight into the behavior of the structure with regards to vibrations.

High rise buildings in the Netherlands are by far not as tall as structures elsewhere in the world. This is caused by several factors from which the main factor is related to the Dutch building regulations. For example, only a maximum depth of 7.2 meters is allowed for offices in day light regulations which leads to smaller surface areas in the Netherlands compared to elsewhere. However, the same aspect ratio for tall buildings is used and thus this leads to lower buildings. Since the sensitivity of a building to vibrations is primarily determined by its aspect ratio, tall buildings in the Netherlands are as sensitive to vibrations as buildings elsewhere. [1;11]

#### 1.1 Relevance of this thesis

The focus in this thesis lies on wind-induced vibrations in high rise structures in the Netherlands. The low frequency vibrations in the building cause accelerations in the building which are sensible for occupants in the building. The accelerations are a measure for the comfort level of the occupants: once the perception threshold of occupants to accelerations is exceeded, the building could be referred to as uncomfortable. This effect increases for the torsional motion since this motion is bilateral. [32;39]

In the structural design phase of a high rise structure the structural designer could estimate the

accelerations of the building by the application of a model. In case the perception threshold is exceeded in accordance with NEN-EN 1991-1-4, auxiliary damping is required. However, structural designers are not yet familiar with the influence of auxiliary damping on the structural system in terms of numerical values.

Adjustments become more expensive in later stages of the design process while the impact on the performance decreases in later stages, see Figure 1.1. From this figure it becomes clear that the vibrational behavior of high rise structures have to be examined in an early stage of the design process to reduce the costs to a minimum and to increase the impact on performances. The study on the vibrational behavior partly requires a research on the damping of the structure: is the damping in the building sufficient to suppress the wind-induced vibrations and its corresponding accelerations to a level which is comfortable for the occupants? If this is not the case, auxiliary damping is required to reduce the accelerations. [22]

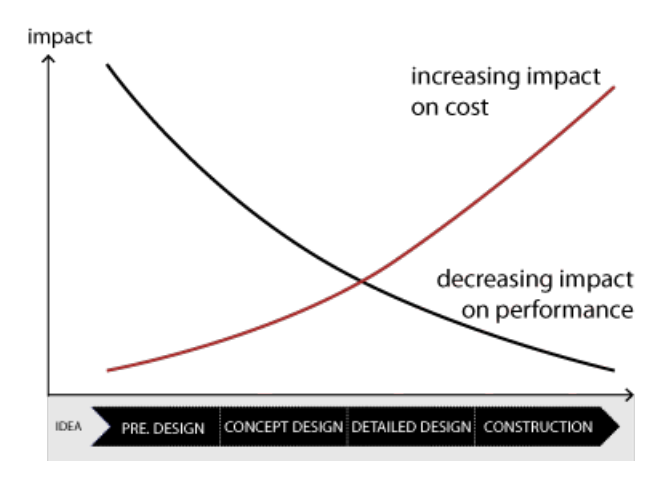


Figure 1.1: Impact of adjustments to the design on costs during the process

Regulations do not provide a quantification of auxiliary damping and its position in the building but expect the structural designer only to know the total value of auxiliary damping. Manufacturers then have to quantify this value into a number of dampers at a certain position in the structure. However, this is a time consuming process and is not suitable for simple first checks, which is desirable in the preliminary design phase of a high rise structure. [29;30]

For practical and aesthetic reasons, the dampers could only be implemented to certain parts of the structure. Not all types of damping systems could be integrated to any position in the structure. One of the damping systems which could be integrated to the structure easily is the viscoelastic damper (VED). Viscoelastic materials (VEMs) are rubber like materials which are partly viscous and partly elastic. Consequently, the energy dissipation from the structure by the VED is caused by storing part of the energy in the VEM and transferring part of the energy to heat. [8;17]

All the above has not been taken into account by the development of current computer programs: the programs do not suffice with regards to the quantification of damping systems in high rise structures and the structural designer is only provided with information regarding the required amount of auxiliary damping. Moreover, an actual required number of dampers and their position is not proposed by the programs. [28]

#### 1.1.1 A prototype tool

The above analysis led to the objective of this thesis:

A feasibility study on the development of a prototype tool to determine the required amount of viscoelastic damping in a high rise structure to reduce accelerations from wind-induced vibrations'

To meet this objective, an analysis has to be executed into the behavior of VEDs in a structure in order to quantify the damping of the discrete damping system. Also, this quantification has to be studied for the theoretical model behind the prototype tool. The set-up of the tool is displayed in Figure 1.2.

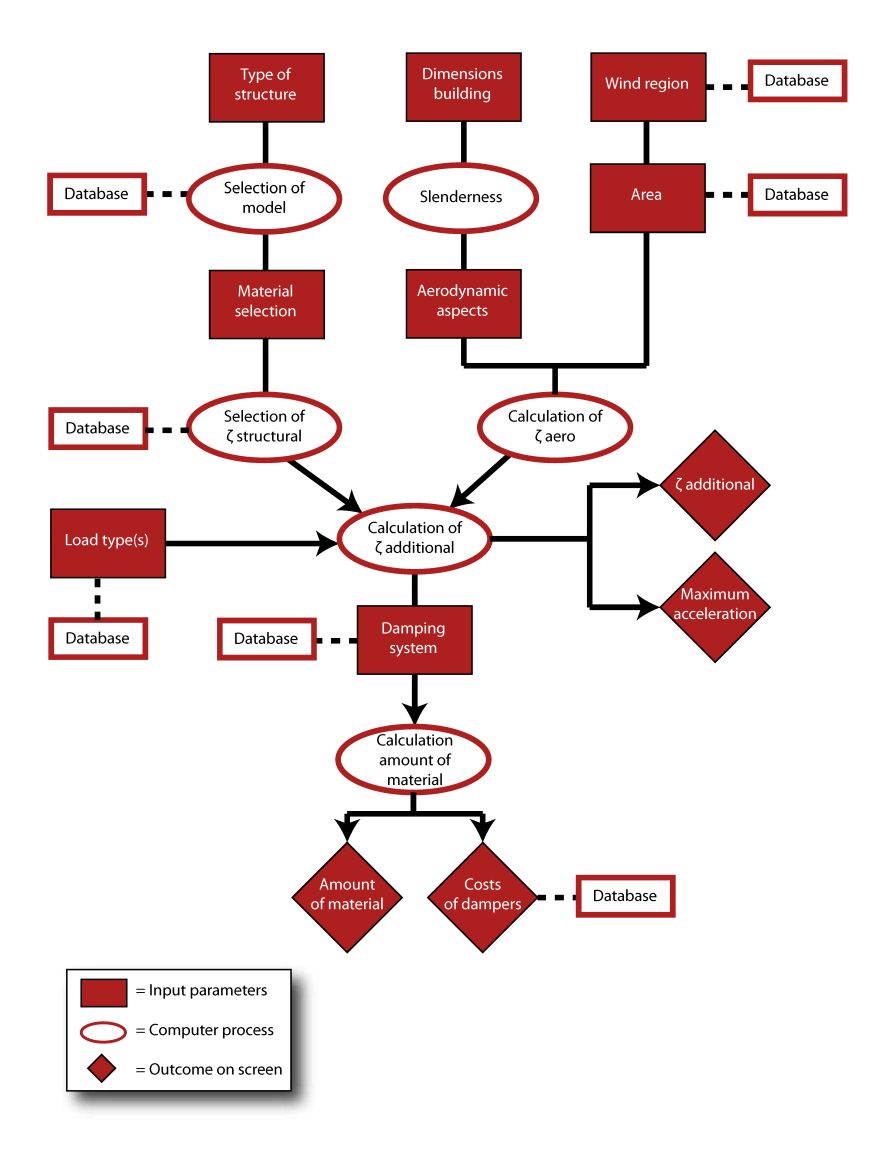


Figure 1.2: Set up model

The squared shaped red boxes are to be adjusted by the structural designer. The structural designer will be able to define the parameters of the structure from simple drop-down menus. The tool will immediately show the result visually and by numbers. This set-up allows the structural designer to adapt his parameters in a later stage of the design. Additionally, the different positions of the damper could be studied to find an optimum between reducing the

accelerations and practical aspects such as the position of a damper.

#### Considerations for the modeling phase

Formulas regarding dynamic wind load in NEN-EN 1991-1-4 are based on a single mass spring damper (1-MSD) system. It is therefore required to create a corresponding dynamical model of a high rise structure which is constructed from multiple MSDs or to find an equivalent 1-MSD to apply the wind load to. The latter option is preferred over the first one because it simplifies calculations. However the latter option will simply calculations, the N-MSD model will be preferred because the modal stiffness, mass and damping can be taken into account and thus this is a better method to model high rise structures. By first programming the N-MSD system, the correctness of the model can be checked for a single situation. Then, the N-MSD can be changed into a parametric model, which is the basis for the prototype tool. The input parameters and formulas for the wind load will be adopted from NEN-EN 1991-1-4.

Next to that, the behavior of the VEM in a structure plays an important role and thus has to be investigated. This will be done by means of a physical test set-up. The aim of this tests was to examine the frequency dependence of the material as well as its behavior in the structure. Layers of VEM with a variation in thickness have been applied to the structure in order to investigate the influence on the stiffness to the structure. The results of the physical test set-up have been used to model VEDs in high rise structures in the N-MSD.

#### 1.2 How to read this report?

This thesis consists of three different parts, namely a literature review, the main report and the appendices. In this report first a brief summary of the literature study will be presented in Chapter 2. The next chapter provides the reader with information regarding the physical test set-up and the results of the tests. In Chapter 4 the definition of a core and braced portal frame structure will be presented. Then, in Chapter 5 the conclusions will be presented of the research as well as some expectations for related topics. Also, recommendations for future research are discussed. The final chapter of this report is a summary of Chapter 5, which should provide the reader a quick insight into the result of this thesis.

Throughout the report references are made to the literature review and appendices. The reader is recommended to consult these reports in case any additional information is required or any background information regarding the topics in this report is desirable.

## 2 Results of literature review

This chapter is based on an extensive literature review which can be found in the report 'Literature study'. The reader is referred to this report for more information on regarding the topics discussed in this chapter.

In this chapter, the results of the literature review are briefly summarized and presented. The purpose of this chapter is to provide the reader with first clarifications and justifications for considerations made in the modeling phase.

#### 2.1 High rise structures

There are several structural systems for high rise structures. The structural systems considered in this thesis are the braced frame structure, see Figure 2.1 and the core structure, see Figure 2.2. These structures are selected for the analysis because the structures are often used in high rise structures. Even a combination of the two structures is often used; this principle will be used for the model of the high rise structure. [12;31;37]

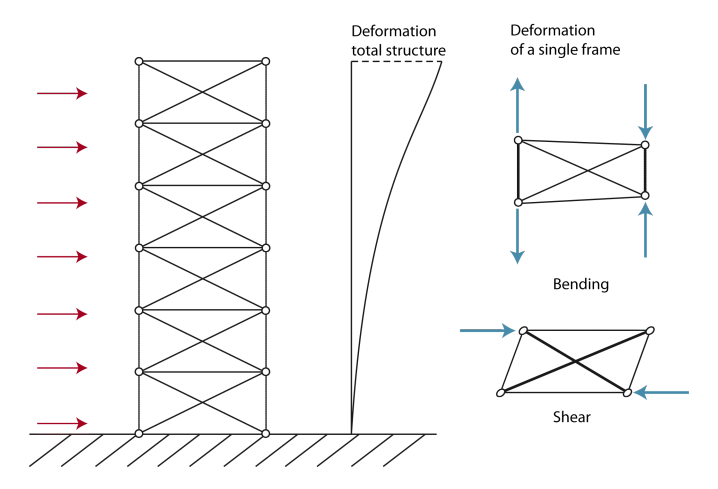


Figure 2.1: Model for a braced frame structure

In braced frame structures the horizontal members are connected to the vertical members by hinges. Diagonal bracings are connected to these hinges for the sake of stability. As demonstrated in Figure 2.1, the vertical members of the frame are loaded by axial forces, which are caused by bending of the structure. Furthermore, the diagonals are activated as a response to shear forces. Thus, the deformation of braced frame structures is a combination of shear and bending deformations.

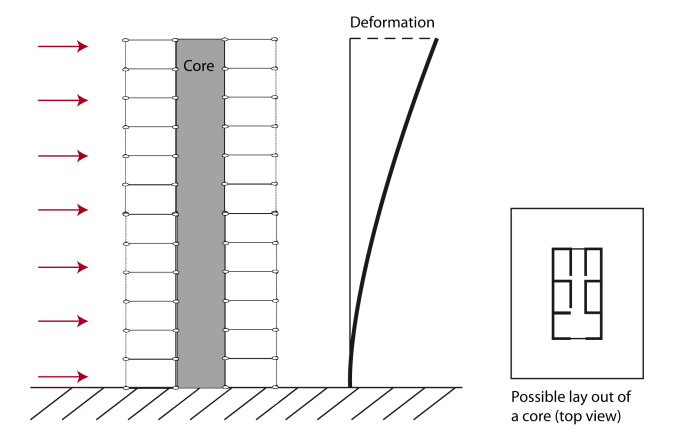


Figure 2.2: Model for a braced frame structure

The core structure type is the type of structure which is mostly applied for high rise structures. Other structural systems are often a coupled system of a core structure and some other extensional structure. A core structure consists of a group of shear walls applied over the height of the building and its deformation is caused by bending, see Figure 2.2. Due to its large bending stiffness, the core provides horizontal stiffness to the building. The attachment of floors and beams to the core also contributes to the stiffness of the overall stiffness.

The height of high rise structures allows for large relative displacements to occur at the top of the building. Consequently, its corresponding relative accelerations could be large as well, which could negatively influence the comfort of occupants in the building. [32;1]

#### 2.2 Dynamic wind load

In this thesis, the accelerations from wind-induced vibrations is studied. Wind loads have a random and unpredictable character which makes regular load cases (such as harmonic ones) not useful in a model. Consequently, regular load cases and models are not applicable for wind loads. Fluctuations of the wind over time are considered random and thus the wind spectrum is referred to as random proces, which comes down to the following: [42;43]

**Definition 2** A random process is an unpredictable function from which the outcome is never the same by any set of initial data.

The total wind load on a building as a whole is equal to the summation of loads on parts of the surface area of the building. In mathematical form this leads to the following set of equations: [9;13]

$$F_w = \sum C_{p,i} A_i q_{w,i} \tag{2.1}$$

$$q_w = \frac{1}{2}\rho v^2 = \frac{1}{2}\rho(\bar{v} + \tilde{v})^2 = \frac{1}{2}\rho\bar{v}^2 + \rho\tilde{v}\bar{v} + \frac{1}{2}\rho\tilde{v}^2$$
(2.2)

In Equation 2.2,  $q_w$  resembles the wind pressure which is stochastically determined by introducing a mean wind velocity  $\bar{v}$  and fluctuating part  $\tilde{v}$  to resemble unpredictable character of the wind, see also Figure 2.3. The fluctuating part of the wind velocity is determined stochastically by introducing a standard deviation for the wind velocity. The standard deviation is dependent on the location of the wind and the environment of the high rise structure.

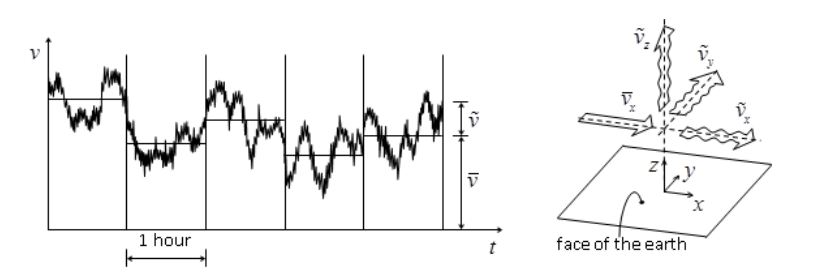


Figure 2.3: Wind spectrum over time (Obtained from Vrouwenvelder, 2004)

Due to the random character of the wind, its corresponding load and response functions of the wind load must be obtained by means of a spectral analysis. The structure of this analysis is presented in Figure 2.4.

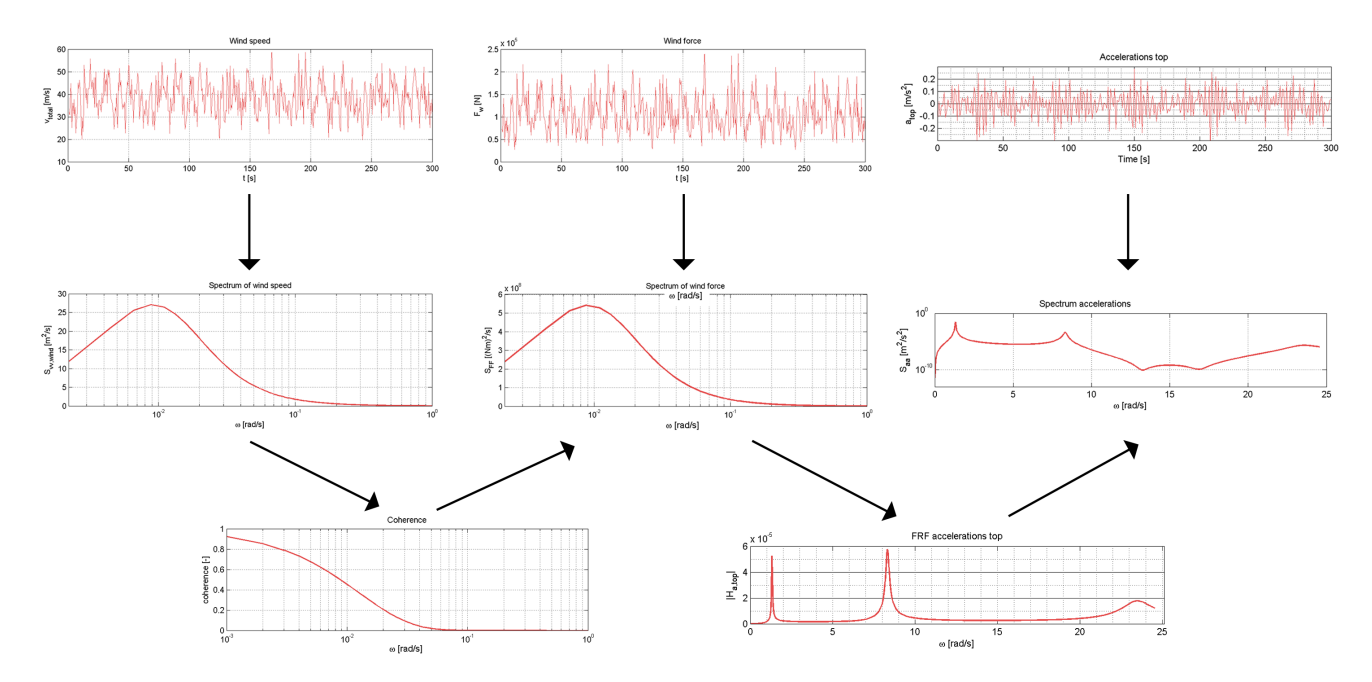


Figure 2.4: Steps to be taken to find dynamic response under dynamic wind load

Wind loads occur in three different directions: along-wind, crosswind and torsional direction. In general, people are more sensitive to torsional wind loads than the other two directions due to the effect of bi-lateral motion. [24]

Although torsional wind loads are most important, in regulations torsional wind loads are considered as displayed in Figure 2.5 (left). However, another model is desired, namely the model in Figure 2.5 (right). This arises from the assumption wind loads on buildings are uniformly distributed across its faces, and the resultant shear force acts in the direction of the wind. However, this is rarely the case since torsional motion is possibly caused by the following causes: [29;39]

- 1. An unequal pressure distribution is caused by the stochastic character of the wind
- 2. Wind acting at a random angle to the building
- 3. Asymmetry in mass and stiffness of the building
- 4. Non-symmetric cross-sections.

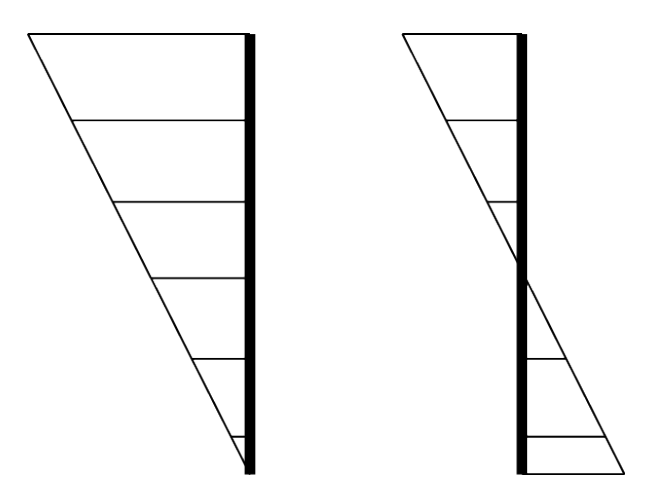


Figure 2.5: Torsion in regulations (left) and desired model (right)

In literature, models for torsional motion are mainly constructed from measurements in wind tunnels and pressure areas at existing buildings. Nevertheless, the ideal situation for the structural engineer would be to have insight into the structure's behavior in the preliminary design phase. In case of unwanted torsional motion of the structure, the design can still be adjusted rather easily in this phase of the building process. In addition to that, measurements in wind tunnels are expensive so an accurate theoretical model is also desirable with respect to the reduction of costs. [24]

If the eigenfrequencies of the torsional and translational motion are about the same, the deformation shape will formed by a summation of both motions. In that case also the velocity and acceleration profile will contain a translational and torsional component. The equivalent acceleration in the along wind direction is found by:

$$a_{equivalent} = \sqrt{a_{along}^2 + a_{torsional}^2} \tag{2.3}$$

In this formula the maximum accelerations for both directions are taken into account but acceleration is reduced by the square root in the above equation.

#### 2.3 Structural dynamics

High rise structures could be modeled as NMSD systems or as a continuous system. The fundamentals of NEN-EN 1991-1-4 regarding dynamic wind load are based on NMSD systems and thus this method will be adopted in this thesis. For a broad description of all available methods, see the Literature study report.

Mathematically, an NMSD system is expressed by the equation of motion:

$$M\ddot{u} + C\dot{u} + Ku = F(t) \tag{2.4}$$

The dynamic stiffness of the structure is then described by:

$$S = K - \omega^2 M + i\omega C \tag{2.5}$$

Then, the transfer function for the displacement is obtained by its inverse  $H_u = S^{-1}$  and the transfer function of the accelerations is described by: [7;26]

$$|H_a| = \omega^2 |H_u| \tag{2.6}$$

The transfer functions will used for the spectral analysis to determine the response of the structure, see Figure 2.4.

#### 2.4 Damping

In this thesis, three types of damping will be considered in accordance with NEN-EN 1991-1-4: [29]

$$\delta_{tot} = \delta_s + \delta_{ae} + \delta_d \tag{2.7}$$

Respectively, this is the logarithmic decrement of the structural, aerodynamic and auxiliary damping of the underdamped system. The auxiliary damping source has the largest impact on the total damping of the system. The logarithmic decrement is related to the damping ratio by the following relation:

$$\delta = \frac{2\pi\zeta}{\sqrt{1-\zeta^2}}\tag{2.8}$$

The general shape of current damping predictor models is shown in Figure 2.6 and in mathematical form as follows: [21]

$$\zeta_s(X) = \zeta_b + \zeta_c(X) \le \zeta_{s,max} \tag{2.9}$$

$$\zeta_c(X) = \beta X^a \le \zeta_{c,max} \quad \text{for} \quad X\epsilon \quad < X_l, X_m >$$
(2.10)

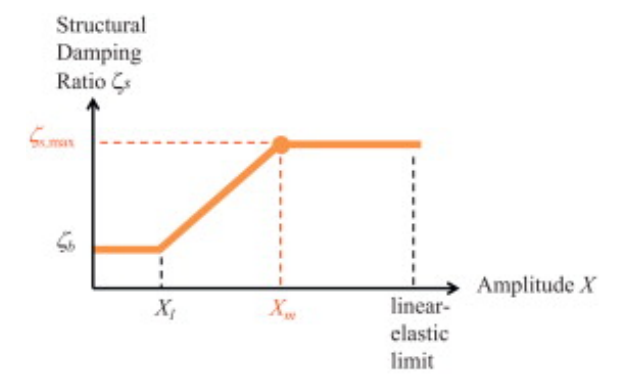


Figure 2.6: General shape of current damping predictor models

In the above equation,  $\zeta_b$  is the base line damping ratio at the low-amplitude plateau. If the amplitudes of vibration are above a certain value  $(X_l)$ , the damping ratio is determined as a nonlinear function of amplitudes of vibration response within a certain range. Once the amplitude  $X_m$  is reached, the damping remains constant at the high amplitude plateau at its maximum  $\zeta_{c,max}$  for  $X \geq X_m$ .

The above damping model can be adopted directly for steady state motions under sinusoidal vibrations. However, in case of random vibrations, the amplitudes of the responses will be varied. By an increase of amplitude the natural frequencies tend to decrease, which is an illustration of the amplitude dependency of the natural frequencies. However, the contribution of this factor to the frequency changes contributes in the third decimal only which suggests that frequency nonlinearity is relatively small for tall buildings and thus for this thesis a linear situation is assumed. [2;21]

As a starting point, three types of passive dampers were considered in this thesis, namely: viscous dampers (VDs), viscoelastic dampers (VEDs) and fricion dampers (FDs). A detailed description of these type of dampers is presented the report 'Literature study'.

2.4. DAMPING 11

The adopted type of damper in this thesis is the VED because VEDs are especially useful in situations where high damping at low frequency is desired. Hence, VEDs are applicable very well to suppress wind-induced motions. Additionally, the damper is easy to integrate into the load bearing structure and the VEM is rather cheap. For instance, in Colombia Center Building VE dampers were only 1.5% of the total building costs. This even included an extensive testing program. VEDs partly store energy from the load bearing structure to the rubber by fluid friction. The other part of the energy is dissipated by elastic energy. However, only 2-4% of the energy is dissipated by fluid friction to the viscoelastic material (VEM). [32;41]

Amorphous polymers behave like glass at low temperatures, while at intermediate temperatures above the glass transition temperature ( $T_g$  in Figure 2.7) the polymer behaves as a rubbery solid. Once the melting temperature  $T_m$  is exceeded, the material behaves as a viscous liquid. For relatively small deformations the mechanical behavior at low temperatures may be elastic and at the highest temperatures viscous behavior occurs. The rubbery solid behavior in the intermediate region is a combinations of these two extreme characteristics and is named viscoelasticity. The (energy) storage capacity of the material is expressed by the storage modulus of the material, which changes by any shift in temperature. In a building, temperature control is required in the surrounding area of the VED for instance by the integration of the VEM with steel members because of the high conductivity of steel. [8]

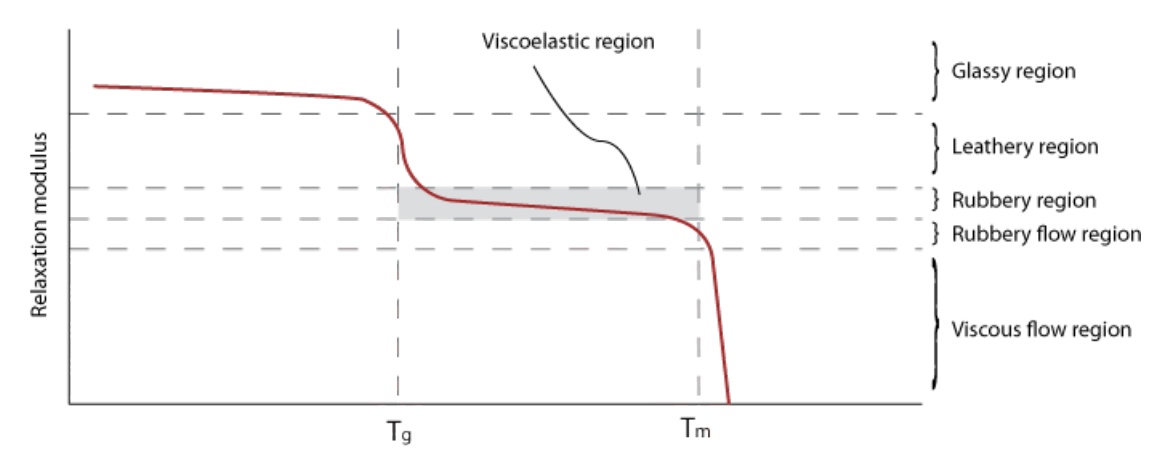


Figure 2.7: Temperature dependence of VEM (Figure based on Callister, 2003)

The ratio between the viscous and elastic part differs for each material and defines the exact behavior of the material. The stress-strain behavior of a fully elastic and viscous material are displayed in Figure 2.8.

The stress-strain behavior lies somewhere in between the two extremes presented in this figure and is indicated by a phase shift,  $\Psi$ .

The most most effective way to dissipate energy from the structure is by shear. The above stress-strain relation also holds for shear. Then, the stress-strain behavior in shear of a VEM is mathematically described by: [17;20]

$$\tau(t) = \tau_{elastic} + \tau_{viscous} = G\gamma(t) + \eta \frac{d\gamma(t)}{dt}$$
(2.11)

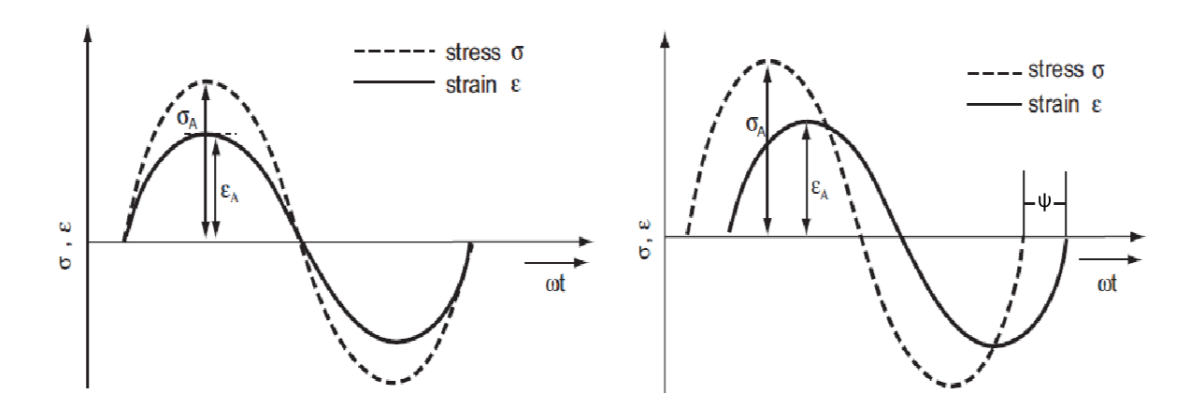


Figure 2.8: Stress-strain relation of an elastic material (left) and a viscous material (right)

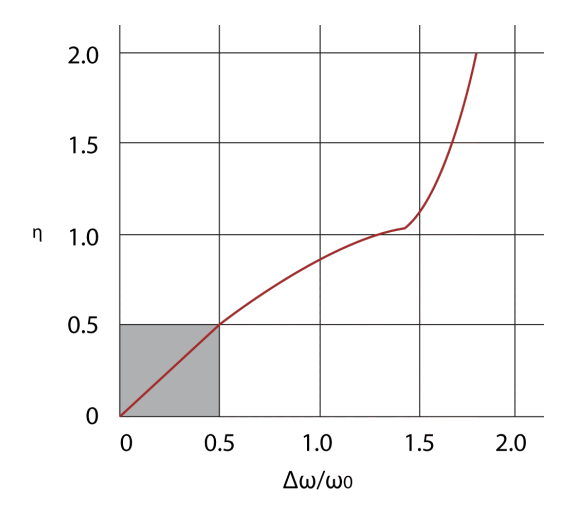


Figure 2.9: Relation of the loss modulus to the damping ratio

Calculations on VEDs are often costly due to the non-linear behavior of the material. Numerical methods are often adopted for calculations on VEMs. However, the behavior can also be described by linear relations, which is the case for small values of the damping ratio, see the gray area in Figure 2.9. In that case, the loss modulus is related directly to the damping ratio and damping coefficient of the VED by: [17;20]

$$\zeta = \frac{\eta}{2} \quad ; \quad c_{VEM} = \eta \frac{K'}{\omega} \tag{2.12}$$

Where K' is the storage modulus of the VEM. The behavior of the VEM becomes non-linear for higher values of  $\zeta$ . In that case, the loss modulus is to be obtained from:

$$\eta = \frac{1 - \left\{1 - 0.5 \left(2\zeta\right)^{2}\right\}^{2}}{s^{2} - 1} \quad ; \quad 2\zeta = \frac{\Delta\omega}{\omega_{n}} \tag{2.13}$$

Where s takes into account the reduction of the amplitude by 1/s from  $\omega_n$  at  $\omega_1$  and  $\omega_2$ . This is the basis of the half-power bandwidth method, which is a method to determine the damping ratio of a structure or material from the frequency respons function, see Figure 1.2.

2.4. DAMPING 13

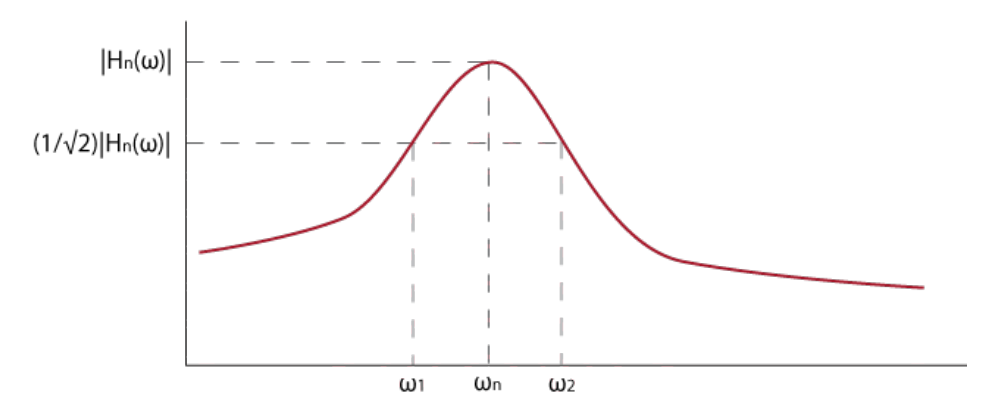


Figure 2.10: Basis of the half-power bandwidth method

In accordance with this figure, the damping ratio is determined by: [45]

$$\zeta = \frac{\omega_2 - \omega_1}{2\omega_n} \tag{2.14}$$

This method will be employed in Chapter 3 to determine the damping in the VEM in the physical test set-up.

#### Hysteresis

The non-linear behavior of the damping material is implemented into the equation of motion as follow:

$$m\ddot{u} + F_{damper}(u, \dot{u}) + ku = F(t) \tag{2.15}$$

This new equation makes calculations more complex since it cannot be solved as a linear differential equation. The force-displacement diagram of a non-linear material is resembled by a loop. The exact shape and size of the loop are dependent on the type of material but form of the hysteresis loop for VEM is displayed in Figure 2.11. The loop is observed by quickly loading and unloading the material, and it is called a hysteresis loop. If such loop is observed, it means the material is stretched more easily during unloading than during loading. This loop applies to harmonically loaded materials and the area enclosed by the loop resembles the energy being dissipated per cycle from the material. More energy is required during loading than during unloading and therefore it holds: [?] b11[3] p.57

$$E_{dissipated} = E_{loading} - E_{unloading} \tag{2.16}$$

In case of a harmonic load  $u = \hat{u} \sin(\omega t)$ , the spring and damping force are described by:

$$F_s = k\hat{u}\sin(\omega t)$$

$$F_d = c\hat{u}\omega\sin(\omega t)$$
(2.17)

The hysteresis loop is commonly used to describe the dampening behavior of a material or damper. The shape of the hysteresis loop of a VED (Figure 2.11) can be explained by the dependency on both velocity and displacement of the material. The viscous part of the material is related to the velocity and the elastic part to the displacement.

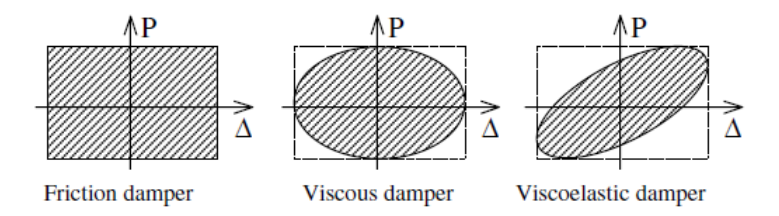


Figure 2.11: Hysteresis loops for different types of dampers

Equivalently, the hysteresis loop can be presented for the  $\sigma - \varepsilon$  relation, see Figure 2.12. It becomes clear from this figure the material damping can be modeled by adding a complex term to the E-modulus. This is an important observation for modeling the portal frame structure in Chapter 4.

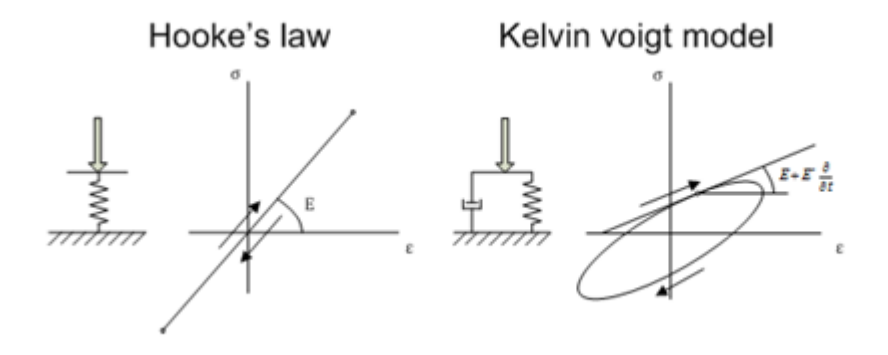


Figure 2.12: Hysteresis loop as  $\sigma - \varepsilon$  relation. (Obtained from Berg, 2012)

# 3 Physical test set-up

In this chapter the set-up, results and interpretations of the results of the physical test set-up will be discussed.

#### 3.1 General description of investigations

Within this thesis, two investigations will be distinguished:

- 1. Investigation on VED
- 2. Investigation on modeling a N-MSD as a basis for the prototype tool

Both investigations are linked since the modeling of the VED has to be implemented into the prototype tool. No literature was found on numerical values of the frequency dependent dynamical properties of specific VEMs. These properties are required to determine the damping of the VEM in a structure. Therefore, it is convenient to make a model which allows to gain insight into the order of magnitude of the numerical values of the dynamical properties of VEMs.

Secondly, it is expected the thickness of the VEM layer in a structure could influence the overall stiffness of the structure. This expectation arises from the analysis of Figure 3.1; the stiffness of the layer of VEM is determined from:

$$F = \underbrace{\left\{\frac{G_{rubber}BL}{t}\right\}}_{\text{Stiffness rubber}} u \tag{3.1}$$

Where the shear modulus  $G_{rubber} = 0.6$  MPa. Hence, an increase of the thickness of the layer of VEM results in a decrease of the stiffness of the VEM. Possibly, this could influence the stiffness of the element in the structure the VEM is applied to.

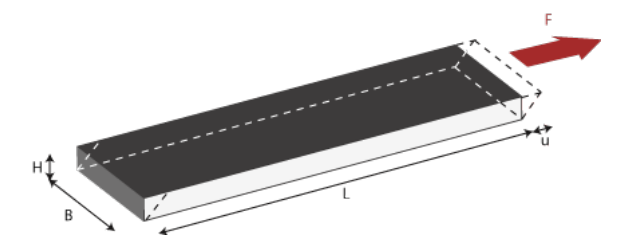


Figure 3.1: Shear deformation of a layer of rubber

Taking into account both aspects, it is convenient to build a physical test set-up of a structure which includes VEDs of different thicknesses to measure the response for different situations.

The measurements could be studied to determine the influence of the VEM layer to the structure and to determine the dynamic and damping properties of the VEM.

The prototype tool will be developed in Matlab. First, an N-MSD system will be modeled to validate the results of the outcome of the model. If the results are correct, then the model will be implemented into the prototype tool.

Beforehand, it was intended to make a comparison of the outcome of the Matlab model and the results generated in Scia Engineer for the same structure and loading situation. However, the dynamic package of Scia Engineer appeared to have limitations with respect to modeling the dynamic load on the structure as well as the response of the structure. Scia Engineer is only suitable to determine the eigenfrequencies of the structure for which it has been used to design the physical test set-up. The initial plan of approach of the modeling phase is presented in Appendix A and the conducted investigation in Scia Engineer is presented in Appendix B.

#### 3.2 Model set-up

A steel braced portal frame structure will be used for the conduction of the experiments. Steel structures are often light weight structures and commonly more sensitive to vibrations then concrete structures. Moreover, braced portal frame structures are often used in high rise structures to stabilize the structure even if the stiffness of the structure is obtained from another structure, such as a concrete core. Therefore, it is expected the results of a test with a braced portal frame are also applicable to other types of other structures.

The test set up must correspond to the conditions of a damped high rise structure subjected to wind load. Hence, vibrations of the structure must be analyzed in the low frequency range. Therefore, the fundamental frequency of the portal frame should be in the low frequency range in order to analyze the behavior of the structure and dampers. Since a fundamental frequency below 1 Hz is hard to obtain for this experiment, the low frequency range is chosen to be larger. Thus, dimensions of the structure are determined from the following relation:

$$f_0 = \frac{\sqrt{k/m}}{2\pi} \approx 1.0 - 6.0$$
Hz (3.2)

As long as the eigenfrequency of the experimental structure is within this range, it is expected the damper's behavior can be properly analyzed.

In Chapter 1 a definition of high rise structures has been presented. Accordingly, a high rise structure is defined by its slenderness, the h/d ratio, which should be 5 or larger. By increasing the height of the building without increasing the size of the floor plan, its stiffness will decrease. To obtain a fundamental frequency within the low frequency range the stiffness should be decreased as much as possible. Therefore, it seems reasonable to find a test set-up which low fundamental frequency is obtained by a slender structure.

#### 3.2.1 Viscoelastic damping

The auxiliary damping system will consist of multiple rubbers because this is an easy way to build a damper. Additionally, rubber is cheap and therefore multiple dampers can be made with a variation in thickness of the rubber. In literature it was made clear that SBR (natural rubber) and EPDM are often used as VED in buildings. [47]

3.2. MODEL SET-UP 17

As was discussed in Chapter 2, the dynamic properties of VEM are frequency and temperature dependent. As for the temperature, a range of 15-35 degrees Celsius is considered. According to literature, the behavior of the SBR will be about the same for each temperature within this range, see Figure 3.2. It is expected this range is applicable to buildings because large changes in temperature usually do not occur due to insulation, heating and cooling devices. As a result, a common temperature range in buildings is 15-22 degrees Celsius, where the exact temperature is dependent on seasonal factors and the regulation of the before mentioned devices. However, the local environment of the SBR layer will be exposed to higher temperatures because of the energy dissipation in the rubber.

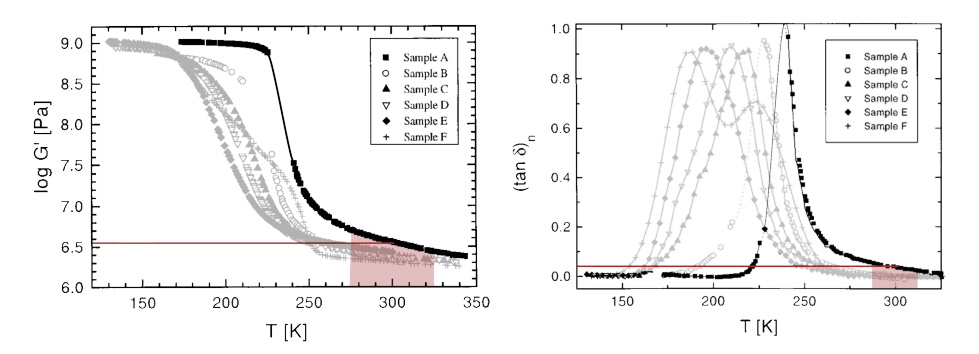


Figure 3.2: Storage modulus (left) and loss factor (right) of SBR as a function of frequency

Additionally, the behavior of each VEM is frequency dependent. Again, any shift in frequency causes a change in storage modulus of the material. In practice, one single operation combines the effects of temperature and frequency into a single variable, which is called reduced frequency.<sup>[17]</sup>

For this thesis, experiments have been conducted to analyze the frequency dependent behavior of SBR in a structure as well as its influence on the response of the structure. Beforehand, it was expected the frequency dependent material properties were representable by similar plot shapes as the temperature dependent properties. Since only the low frequency range is of interest with regards to structures subjected to wind load, the frequency dependent damping of the rubber is best to be analyzed in a range of 0.01-25 Hz.

#### 3.2.2 Design of the portal frame structure

In buildings, H-shaped profiles are often used for columns in case the load bearing structures is erected from steel elements. Therefore, this was the starting point for determining the shape and size of the elements and portal frame structure. Because the first set up was too stiff to reach the low frequency domain, the structure was adjusted. Eventually, the braced portal frame structure is constructed from T-shaped profile columns, strip shaped beams and bracings with a circular cross section. The entire process of determining the dimensions of the frame and the actual construction is presented in Appendix C. For an impression of the set-up, see Figure 3.4.

The structure was hit with a hammer at the top of the frame to introduce an impact force to the structure. The response of the structure was measured for the structure with and without SBR. Two different layers of SBR were analyzed, namely SBR with dimensions 20x25x3 mm (SBR3) and SBR with dimensions 20x25x5 mm (SBR5). These layers were connected to aluminum in the bracing so the layers would be loaded by shear, see Figure 3.3.

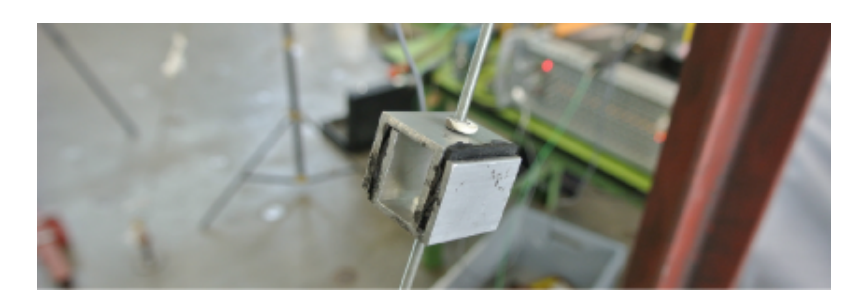


Figure 3.3: Damper of SBR in the bracing of the test set-up



Figure 3.4: Test set up in the lab

#### 3.2.3 Conduction of the tests

The experiments were divided into different 'runs'. Within each run, the test was conducted multiple time. The result of each run is the average of the measurements obtained from each of these tests. A schematic overview of the test set-up is presented in Figure 3.5. In correspondence with this figure, each test consisted of the following steps:

- Step 1: Hit the structure with a hammer near accelerometer 1
- Step 2: Measure the response of the structure from each accelerometer
- Step 3: First verification of the results of each run by analysis on the computer

A detailed description of the steps taken for the execution of the experiment is in Appendix C. Also, a log book of from the tests is presented in this appendix.

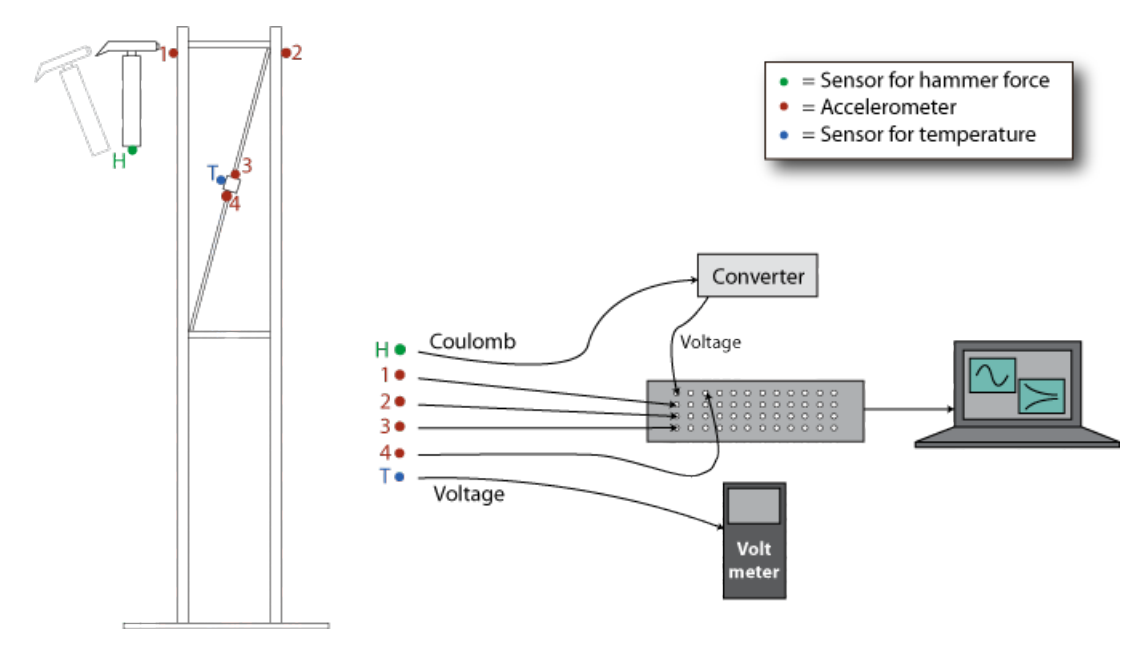


Figure 3.5: Schematic overview of the test set-up

The consistency of the results of each run is resembled by the coherence of a run, see Definition 3.

**Definition 3** The coherence of a run is defined as the similarity and consistency between the measurements taken from different tests within a run.

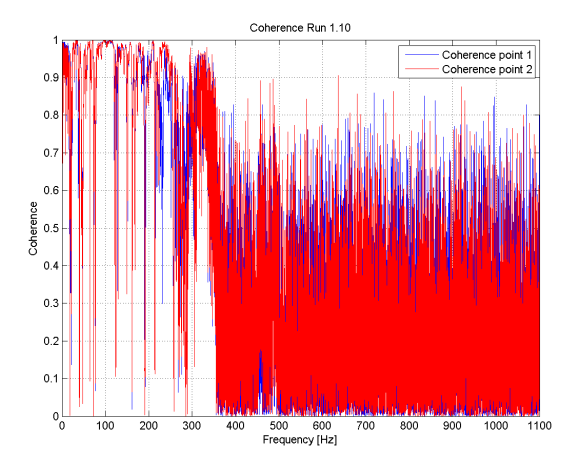


Figure 3.6: Coherence of Run 1.10

In case of full coherence, the coherence equals one. Otherwise, the coherence is between zero and one. An example of a plot of the coherence of Run 1.10 is displayed in Figure 3.6. As is displayed in Figure 3.6, the coherence is between 0.8 and 1.0 in the frequency range of 1.5 Hz to 100 Hz, which makes measurements outside this range not useful. However, the range of 1.5-100 Hz is too wide since only the low frequency range is of interest for this thesis.

**Note:** the range of 0.001-1.5 Hz will not be examined due to a lack of coherence.

#### 3.2.4 Other models of the structure

The braced portal frame structure is modeled with hinged connections between the members. This is displayed by the circles in Figure 3.7.

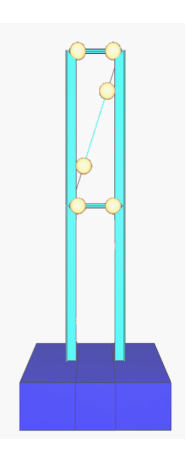


Figure 3.7: Model for experiments in Matrixframe

The dimensions of the frame are displayed in Figure 3.8 (left). In order to determine the stiffness and behavior of the frame, a point load of 1 kN has been applied to the structure, see Figure 3.8 (right).

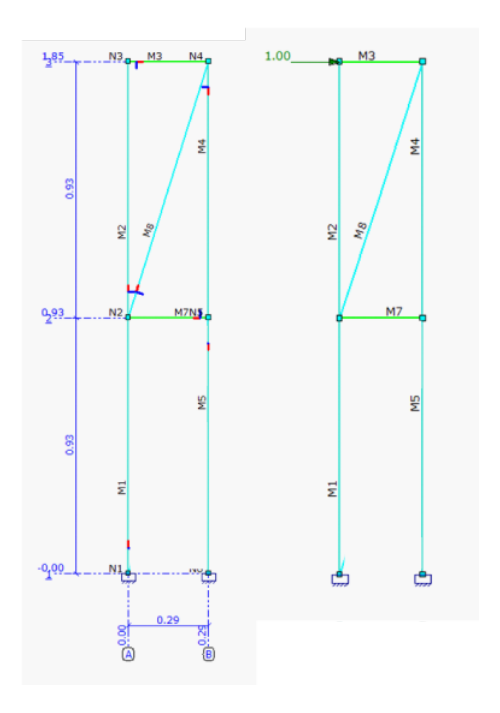


Figure 3.8: Dimensions of the frame (left) and load on the structure (right)

The structure is welded to the floor plate. The strength of the connection is unknown and therefore two situations (and thus two models) are considered with respect to the welds:

- 1. The welds rigidly connected the structure to the floor plate
- 2. The welds connect the structure to the floor plate by simple supports

3.2. MODEL SET-UP 21

In accordance with Matrixframe, if rigid supports are considered, the displacement at the top becomes 0.024 meters, see Figure 3.9A. The input of the model is presented in Appendix D. The stiffness of the frame becomes:

$$k_A = \frac{F}{u} = \frac{1000}{0.024} = 41667 \text{ N/m} = 4.17 * 10^4 \text{ N/m}$$
 (3.3)

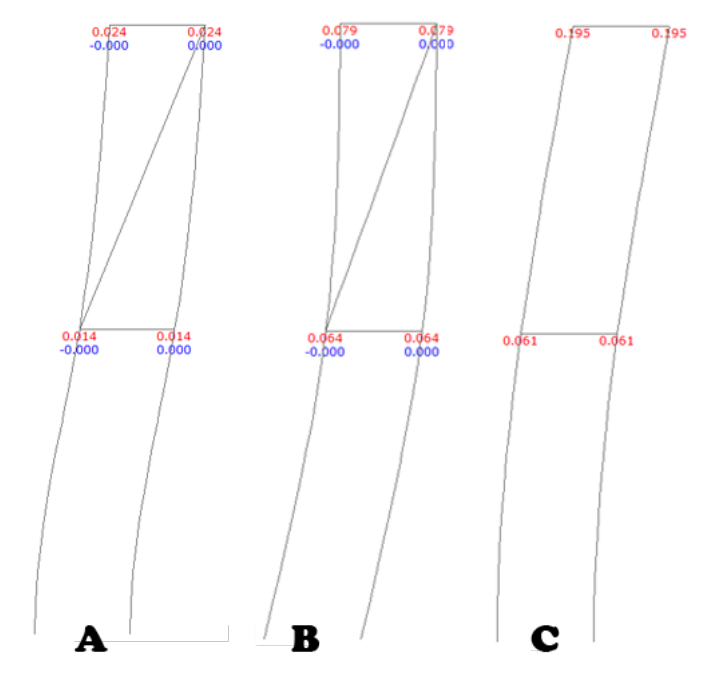


Figure 3.9: Deformation of the portal frame structure rigidly connected to the ground with lower bracing attached (A) and without lower bracing (B)

In case the welded connections at the bottom of the columns are modeled as simple supports, the displacement at the top increases, see Figure 3.9B. The stiffness of the frame becomes:

$$k_B = \frac{F}{u} = \frac{1000}{0.079} = 12658 \text{ N/m} = 1.27 * 10^4 \text{ N/m}$$
 (3.4)

The influence of the bracing on the stiffness of the structure is investigated by the introduction of Model C where the columns are rigidly connected to the ground and the bracing is removed from the structure, see Figure 3.9C. Correspondingly, the stiffness of the frame without bracing becomes:

$$k_C = \frac{F}{u} = \frac{1000}{0.195} = 5128 \text{ N/m} = 0.51 * 10^4 \text{ N/m}$$
 (3.5)

Then it holds that:

$$\Delta k = k_A - k_C = 4.17 * 10^4 - 0.51 * 10^4 = 3.66 * 10^4 \text{ N/m}$$
(3.6)

This is the contribution of the bracing to the lateral stiffness of the structure. Hence, the lateral stiffness of the structure is increased tremendously by the application of the bracing. This also becomes clear from Figure 3.9, where the deformation shape in Model A is different from the shape in Model C due to the application of the bracing. The unbraced portal frame structure in Model C may be modeled as a 1-MSD:

$$m_{eff}\ddot{u} + c_s\dot{u} + k_s u = F(t) \tag{3.7}$$

The bracing in Model A provides lateral stiffness to the frame but is not positioned horizontally. Additionally, it only provides stiffness to the upper part of the portal frame structure; the lower part is still an unbraced structure. In this case, additional damping could have been provided by the connection of the bracing to the column where frictional forces occur. Then, the bracing changes into the left model displayed in Figure 3.10. The stiffness and damping of the connections may be assumed governing if it holds:

$$k_{bracing} = \frac{EA}{l} >> k_{connection} \quad ; \quad c_s >> c_{connection}$$
 (3.8)

Then, in accordance with Appendix E, an operator  $O_b$  is introduced to describe the stiffness and damping elements in the bracing:

$$O_b = \frac{1}{\frac{2}{k_{conn} + c_{conn}\frac{d}{dt}} + \frac{1}{k_{bracing}}} = \frac{1}{\frac{2}{k_{conn} + c_{conn}\frac{d}{dt}}} = \frac{k_{conn} + c_{conn}\frac{d}{dt}}{2}$$

$$(3.9)$$

This operator can be implemented into the equation of motion to find the behavior of the portal frame structure:

$$m_{eff}\ddot{u} + c_s\dot{u} + (k_s + O_b)u = F(t)$$
 (3.10)

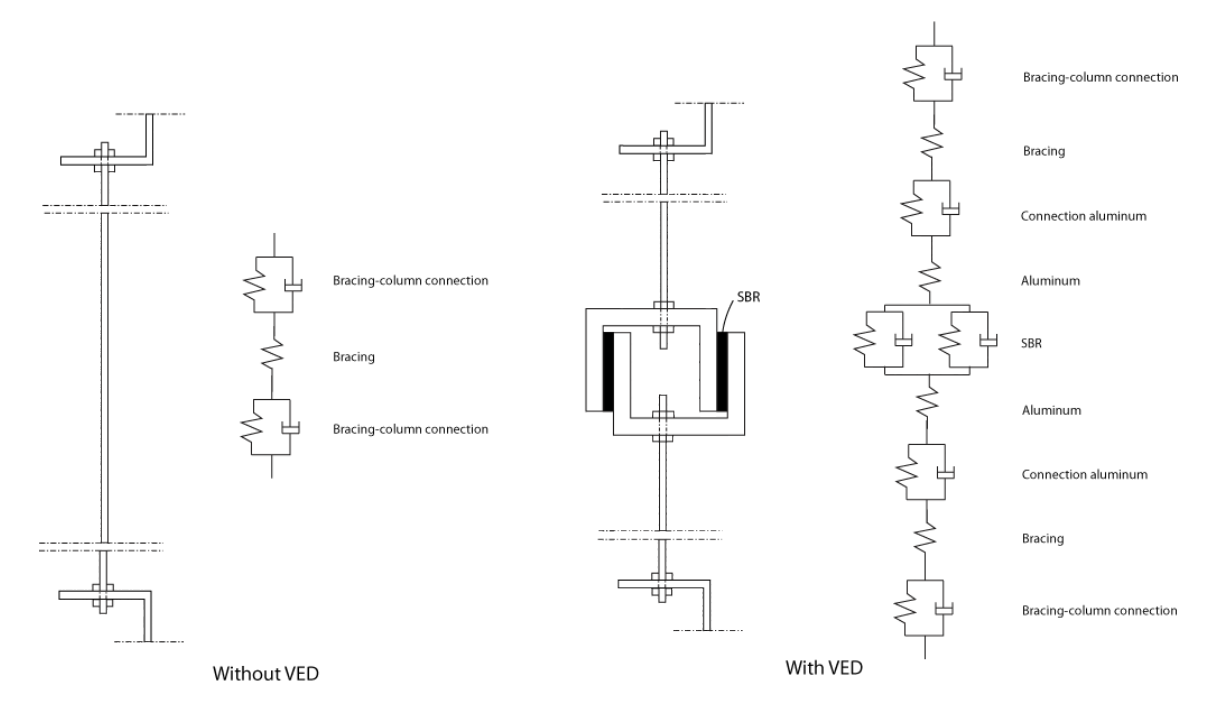


Figure 3.10: Model of the bracing with and without VED

In the physical test set-up, VED was added to the bracing. Then, the model for the bracing changes into the right model displayed in Figure 3.10. Since this model is rather complex, it is convenient to determine what factors could be neglected in the above model. First, the shear stiffness of the SBR layers will be determined. In accordance with Figure 3.11 and Equation 3.1 the shear stiffness of a single layer of SBR5 is:

$$k_{SBR5} = \frac{G_{SBR5}A}{t} = \frac{0.6 * 10^6 * 0.025 * 0.02}{0.005} = 6 * 10^4 \text{ N/m}$$
 (3.11)

3.3. RESULTS 23

And the bending stiffness of the aluminum part is:

$$w = \frac{Fl^3}{192E_{al}I} \longrightarrow k_{al} = \frac{192E_{al}I}{l^3} = 1000 * \frac{192 * 69000 * \frac{1}{12}(17)(2)^3}{25^3} = 9.6 * 10^6 \text{ N/m}$$
(3.12)

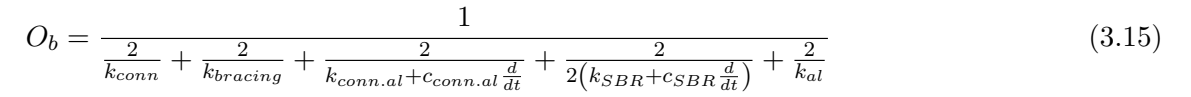
The stiffness of the bracing is:

$$k_b = \frac{2E_{steel}A}{l} = 1000 * \frac{2 * 210000 * \pi * (1.5)^2}{\sqrt{290^2 + 925^2}} = 3.06 * 10^6 \text{ N/m}$$
 (3.13)

Then, the operator  $O_b$  changes into:

$$O_b = \frac{1}{\frac{2}{k_{conn} + c_{conn} \frac{d}{dt}} + \frac{2}{k_{bracing} + c_{bracing} \frac{d}{dt}} + \frac{2}{k_{conn.al} + c_{conn.al} \frac{d}{dt}} + \frac{2}{2(k_{SBR} + c_{SBR} \frac{d}{dt})} + \frac{2}{k_{al}}}$$
(3.14)

Additionally, it may be assumed that the damping provided by the bracing-column connection is much lower than the damping provided by an auxiliary damping component. If this would not be the case, the damping component would not have to be introduced. The damping in the connection of the damping component to the bracing is not being neglected. Therefore, the above equation reduces to:



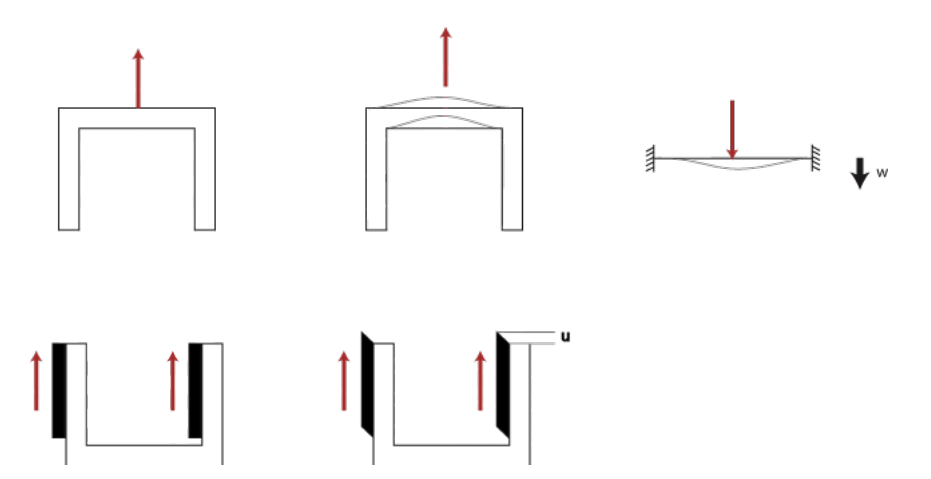


Figure 3.11: Model of the VED

#### 3.3 Results

In this section, an analysis will be conducted of the measurements taken from the physical test set-up. Firstly, a summary of the analysis on the fundamental frequency is presented to point out what aspects in a structure influence the global damping of the structure. Then, the damping obtained from the damping component including SBR layers will be determined. All Matlab scripts concerning this section are presented in Appendix F.

## 3.3.1 Stiffness of the portal frame structure

For each model, the fundamental frequency has been calculated with the above stiffness and the mass of the structure. The effective mass of the structure is estimated to be:

$$m_{eff} = m_{lead} + 0.5 * m_{frame} = 80 + 0.5 * (2 * 1.85 * 3.72 + 6.236) = 90 \text{kg}$$
 (3.16)

An analysis on the fundamental frequency will be presented in the next section. The fundamental frequencies of the Matrixframe models from Section 3.2 are displayed in Table 3.1.

Table 3.1: Fundamental frequencies of different models

Model	$\omega_0  [\mathrm{rad/s}]$	$f_0[Hz]$
A	21.53	3.43
В	11.80	1.88

The fundamental frequency for the undamped frame was measured at 2.48 Hz, which lies in between the values calculated in Table 3.1. Therefore, the connections of the frame structure to the floor plate were somewhere between a rigid and simple supports.

By the relation  $k_0 = \omega_0^2 m_{eff}$  the stiffness of the fundamental frequency has been calculated for Model 1 to 3, see Table 3.2.

Table 3.2: Stiffness at the fundamental frequency of different models

Model	$f_0$ [Hz]	$\omega_0[rad/s]$	$k_0[N/m]$	
1	2.484	15.607	21923	
2	2.450	15.394	21328	
3	2.484	15.607	21923	

The frame stiffness has been calculated with Matrixframe in Section 3.2. Accordingly, it was expected the actual stiffness of the frame would be:

$$1.27 * 10^4 \text{N/m} \le k_{measurements} \le 4.17 * 10^4 \text{N/m}$$
 (3.17)

Where the difference in stiffness is dependent on the supports of the portal frame structure. The values presented in Table 3.2 indeed meet the expectation from Equation 3.17. The structure was designed to be fully clamped by the welded connections but the above implies the structure was not fully clamped to the foot plate. It becomes clear that the stiffness of the structure is highly influenced by executional factors of the set-up of the structure.

The above analysis results in the following conclusions regarding the portal frame structure:

- The connections of the frame structure to the floor plate were somewhere between a rigidly and simple supported connection
- Executional aspects highly influence the stiffness of the structure

## 3.3.2 Analysis of the portal frame structure

First, an analysis is conducted the the fundamental frequency of the portal frame structure to determine the factors that influence the damping of the structure. Beforehand, the fundamental

3.3. RESULTS 25

frequency was calculated to be approximately 5.2 Hz. However, the fundamental frequency turned out to be 3.0 Hz at first and later, after the structure was slightly changed,  $f_0=2.5$  Hz. The difference is occurred because the actual set-up was somewhat different from the initial design. For instance, the structure was not entirely erected from steel but also from aluminum parts. For an in-depth description of the construction of the frame, see Appendix C.

A summary of the analysis on the fundamental frequency is listed below and the complete analysis is presented in Appendix C:

- The natural frequency significantly reduces in case the bolts of the beam-column connection were set less tight, see Figure 3.12
- The tightness of the bolts in the bracing-column connection determines how much load is transferred to the bracing. Consequently, the contribution of the bracing to the global damping is dependent on the same matter
- The connection of the bracing (see Figure 3.13) had to be stiffened because it was vibrating in the transverse direction and thus did not contribute to the global damping in the longitudinal direction.
- In order to reduce the fundamental frequency, the lower bracing was removed as well. Indeed the frequency got lower. However, the damping was decreased as well
- No difference in temperature was measured
- The mass of the portal frame was not changed and thus any shift of the FRF ( $\Delta f$  in Figure 3.14) is caused by a change in stiffness

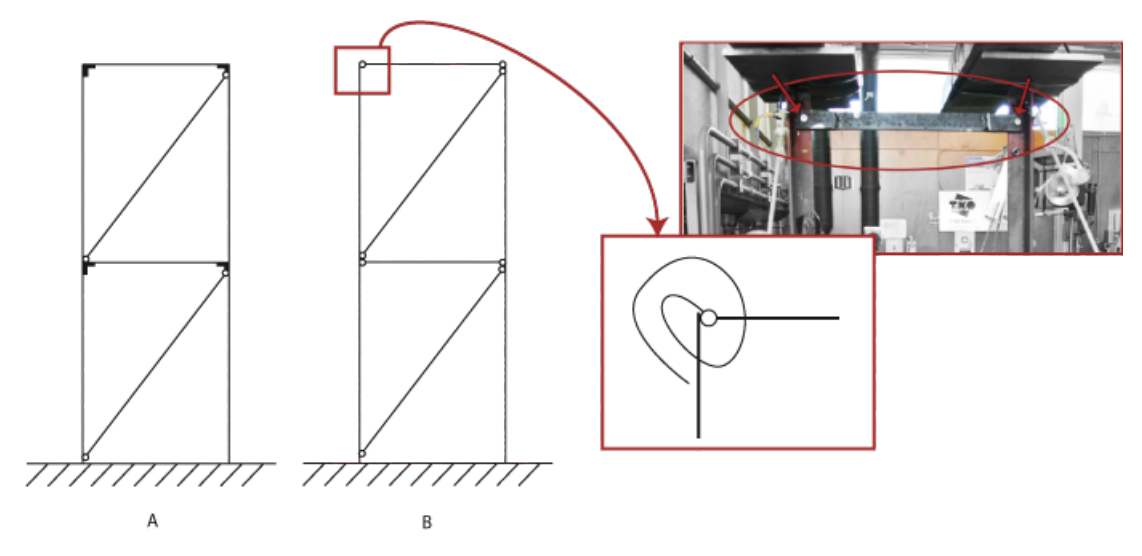


Figure 3.12: Bolts in beam-column connection



Figure 3.13: Aluminum part in bracing-column connection before (left) and after(right) stiffening

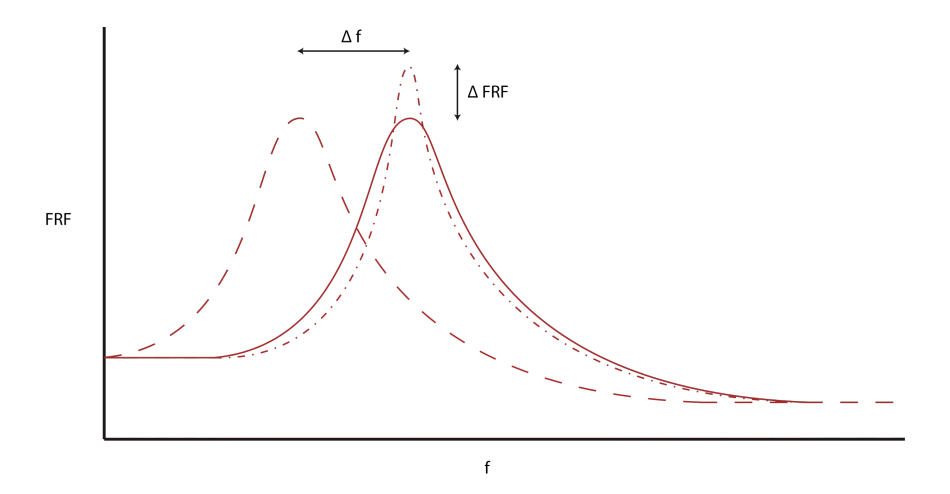


Figure 3.14: Shifting and enlargement of FRF

## 3.3.3 Determination of the damping ratio

The damping ratio can be determined from the FRFs of the tests and from the time signal. Both methods will be presented in this section.

## Frequency response function

The FRFs of the tests are studied in order to determine the frequency dependent behavior of the SBR layers and the braced portal frame structure. Adoption of the half-power bandwidth method results in a corresponding damping ratio per eigenfrequency for each considered model:

- Model 1: the undamped braced portal frame structure
- Model 2: the braced portal frame structure with SBR3 applied to the bracing
- Model 3: the braced portal frame structure with SBR5 applied to the bracing

3.3. RESULTS 27

The FRF near the fundamental frequency of these models is displayed in Figure 3.15 (top) and the corresponding damping ratios are presented in Figure 3.16. The peak in the FRF of Model 2 in Figure 3.15 is shifted slightly to a lower frequency compared to the peaks from Model 1 and Model 3. Since the mass of the structure has been the same for each model, this implies a reduction in stiffness for Model 2. The peaks from Model 1 and Model 3 are located at the same position, which implies the stiffness has not been changed by the application of SBR5. The peak for Model 2 is somewhat lower than the peak of Model 1. However, the width of the peaks is about the same.

From Figure 3.16 it becomes clear that the damping ratio of Model 1 is lowest and the damping ratio of Model 3 is highest. However, the plateau shaped peak of Model 2 requires some extra attention. Why is the top of the peak formed by a plateau? It is likely the actual fundamental frequency is somewhere between the two measured points that form the plateau. Hence, the step size between the two points could be too large which may have caused errors in the results. The plateau implies a wide peak and consequently a high damping ratio. A smaller step size might also give different results for Model 1 and 3. Hence, the obtained fundamental frequencies and corresponding damping ratios could differ from the current values. Therefore, another method will be employed to check the accuracy of the values, this will be done in the next section.

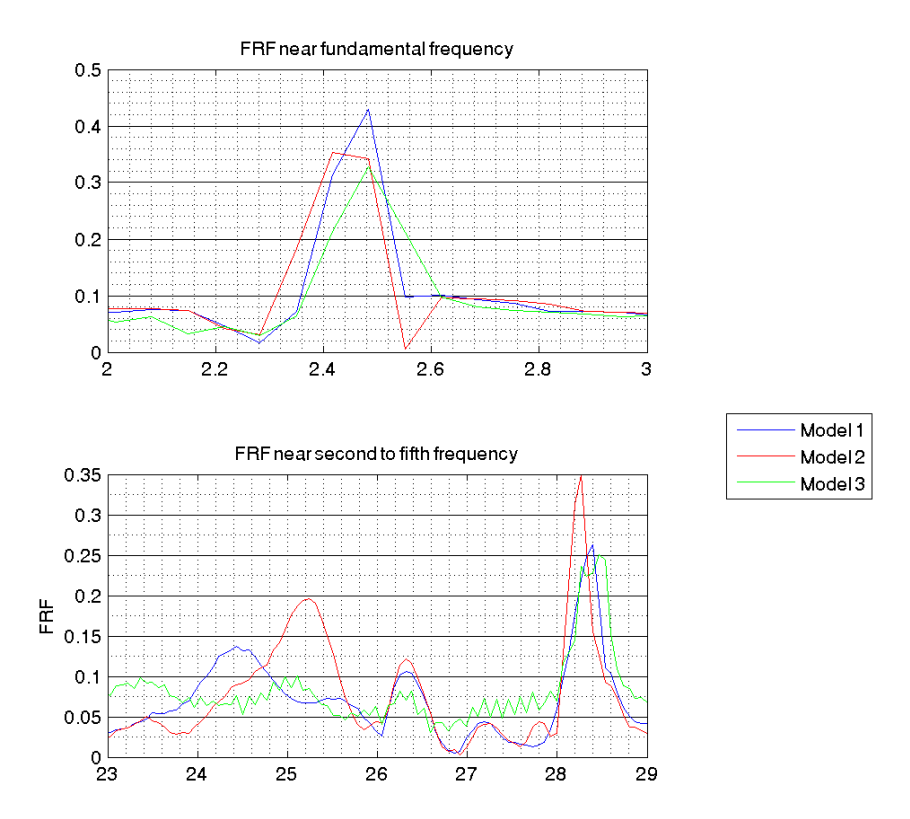


Figure 3.15: The FRFs of Model 1,2 and 3 near the fundamental frequency (top) and near the second to fifth eigenfrequency (bottom)

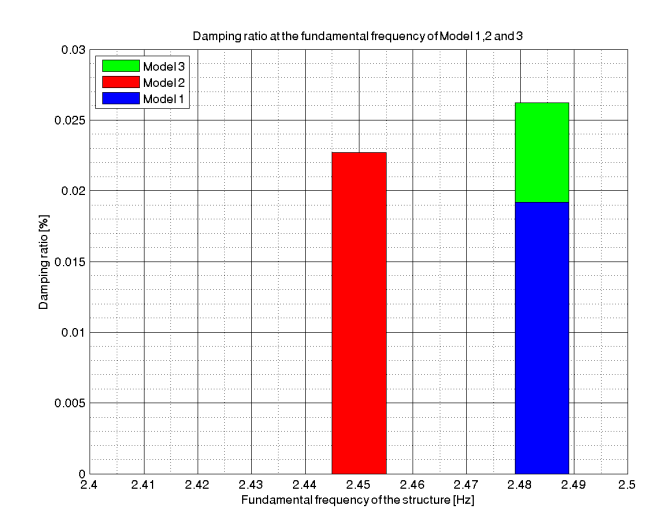


Figure 3.16: Damping ratio at the fundamental frequency of Model 1,2 and 3

Analysis of the frequency dependence of the damping ratio requires a study of the higher frequencies in the FRFs, see Figure 3.15 (bottom). The second to fifth eigenfrequency are located closely together: the second eigenfrequency of Model 1 is lower than the second eigenfrequency of Model 2 and 3. This implies a decrease in stiffness for Model 1, which does not meet the expectations: the rubber in Model 2 and 3 is expected to cause a decrease in stiffness of the structure for higher frequencies. Study of the higher eigenfrequencies does meet the expectations: the  $5^{th}$  eigenfrequency of Model 1 is higher than the  $5^{th}$  eigenfrequency of Model 2 and 3, the structure including the rubber.

The above analysis leads to the conclusion the measurements for higher frequencies than the first are not useful for further analysis because the signal is disturbed. This is probably caused by the step size of the frequencies, which was 0.07 Hz. In future research the tests could be conducted with a smaller step size between the measured frequencies, which should result in a more clear signal for higher frequencies. Additionally, the peak of Model 3 in the FRF in Figure 3.15 could be approximated better as well.

## Time signal

In the previous section has been discussed if the obtained values for the damping ratio and eigenfrequencies are adequate. This is questionable and thus another method than the half-power bandwidth method will be employed to check the adequacy of the obtained values. For each model, the damping ratio will be determined again, this time from the time signal. First, the fundamental frequency has been determined in accordance with Figure 3.17 through:

$$f_0 = \frac{1}{x_j - x_i} \tag{3.18}$$

See the third column in Table 3.3. The obtained values come close to the values found in the FRFs, see the second column in Table 3.3. Therefore, the values for the damping ratios obtained from the FRF and time signal may be compared.

3.3. RESULTS 29

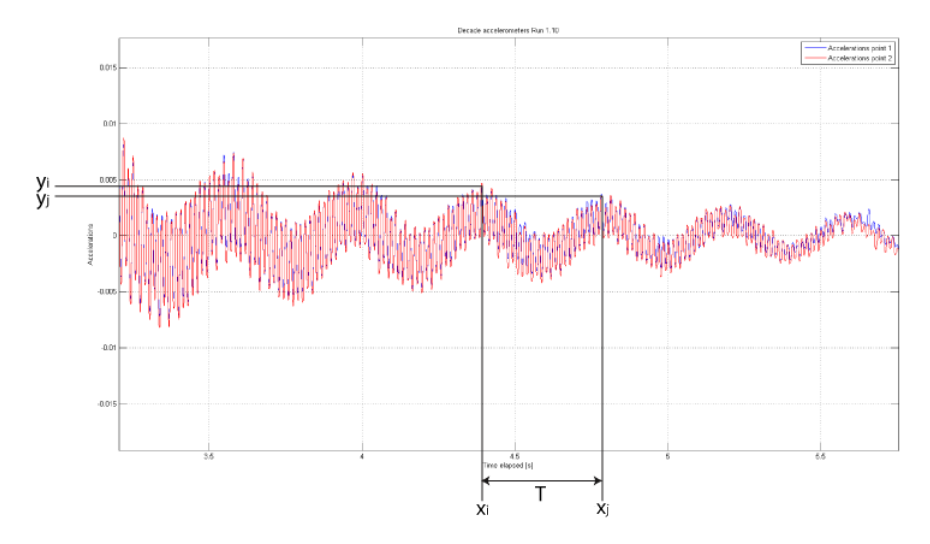


Figure 3.17: Principle of logarithmic decrement

In correspondence with Figure 3.17, the damping ratio for the fundamental frequency is determined from the logarithmic decrement:

$$\zeta = \frac{1}{\sqrt{1 + \left(\frac{2\pi}{\ln\left(\frac{y_i}{y_j}\right)}\right)^2}} \tag{3.19}$$

Where  $y_i$  is the amplitude of a certain peak in the time signal and  $y_j$  is the amplitude of the next peak in the time signal. This method has been adopted for the three models, from which the result is presented in the fifth column of Table 3.3. The values in this column differ from the values found through the application of the half-power bandwidth method, see the fourth column in Table 3.3. However, the values are of the same order of magnitude which makes the half-power bandwidth method a valid approach of the damping ratio.

Table $3.3$ :	Damping	ratios from	the time	signal for	the three	models

Model	$f_{0,FRF}[Hz]$	$f_{0,time}[Hz]$	$\zeta_{FRF}$	$\zeta_{time}$
Undamped frame	2.484	2.482	0.0192	0.0212
Frame with SBR3	2.450	2.463	0.0262	0.0299
Frame with SBR5	2.484	2.476	0.0227	0.0240

### Discussion

The exact calculations of the damping ratio through the half-power bandwidth method are based on FRFs constructed from points located at  $\Delta f = 0.067$ Hz apart. This step size is rather large, which makes the shape of the FRF and thus the obtained damping ratios, questionable.

The damping ratio has also been calculated by the logarithmic decrement method. The time signal is constructed from points located at  $\Delta t = 0.001$ s apart, which is accurate. However, the signal of the fundamental frequency is disturbed by higher frequencies and thus the peaks  $y_i$  and  $y_j$  had to be estimated accurately.

The calculated values for the damping ratio for both methods are different but are of the same order of magnitude. The second method is more trustworthy than the first method because of the step size of the measurements.

For the calculation of the fundamental frequency, the first method is more reliable than the second one except for Model 2 because of the plateau-shaped peak in the FRF (Figure 3.15). Hence, the results of this test remain questionable.

For further calculations the following will be assumed:

- The fundamental frequency of Model 1 and Model 3 are  $f_0 = 2.484 \text{Hz}$
- The damping ratios of the time signal will be assumed for Model 1 ( $\zeta=0.0212$ ) and Model 3 ( $\zeta=0.0240$ )
- The result of Model 2 is questionable

## 3.4 Comparison of theory and practice

In the section the outcome of the test set-up will be compared to the theoretically calculated outcome.

## 3.4.1 Determination of the damping coefficient

The damping coefficient of the fundamental frequency is calculated by the adoption of the relation  $c_d = \zeta 2\sqrt{k_0 m_{eff}}$ , see Table 3.4 and Figure 3.18. Now, the loss factor of the structure can be determined through: [17;40]

$$\eta_0 = \frac{\omega_0 c_0}{k_0} \tag{3.20}$$

The results are displayed in Table 3.4. It is convenient to conduct an analysis on the damping obtained by the application of the SBR layers. Therefore, the behavior of the undamped structure must be compared to the behavior of the damped structure for the fundamental frequency. However, the fundamental frequency of Model 2 deviates from the fundamental frequency of the undamped frame (Model 1). Hence, Model 2 will not be considered for this analysis and thus only the SBR layer of 5 mm thick (Model 3) will be considered.

Table 3.4: Damping coefficients and loss factors of different models

Model	$f_0$ [Hz]	$\omega_0[rad/s]$	$c_{d,0}[Ns/m]$	$\eta_0[-]$
1	2.484	15.607	53.938	0.0384
2	2.450	15.394	62.900	0.0454
3	2.484	15.607	73.603	0.0524

In correspondence with Table 3.4, the damping coefficient  $c_d$  is increased by 73.603 - 53.398 = 19.665 Ns/m by the application of the auxiliary damping component including SBR5. The component is displayed in Figure 3.19A. Also, the loss factor  $\eta$  is increased by 0.0524 - 0.0384 = 0.014. This implies an increase of the damping to the structure by the application of SBR5. However, the exact damping coefficient by the layers of SBR remains still unknown. This will be explained below.

The damping system in the bracing has been modeled as a parallel system with the stiffness of the structure. However, this would only be the case if the bracing would not provide stiffness to the structural system. In Section 3.2.4 has been calculated that the stiffness of the bracing was about 87.8% of the stiffness of the structure. Hence, the damping system is not in parallel with the stiffness element of the structure but a combination of a series and parallel system. This has also been presented in Section 3.2.4. The total damping of the structure was determined to be:

$$c_{tot,undamped} = 53.398 \text{Ns/m} \tag{3.21a}$$

$$c_{tot,damped} = 73.603 \text{Ns/m} \tag{3.21b}$$

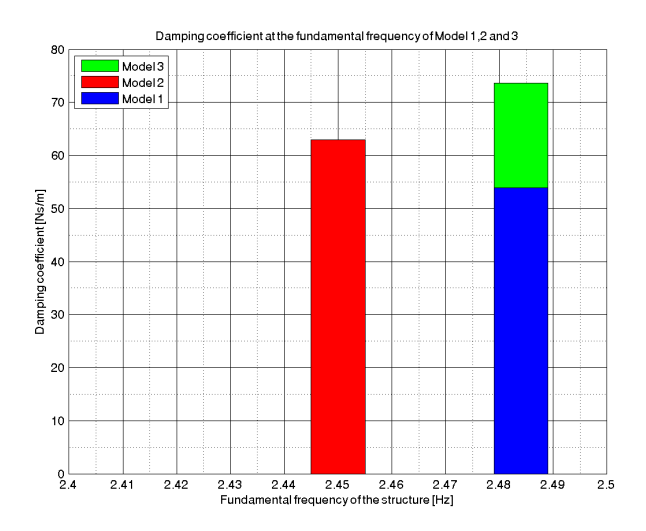


Figure 3.18: Damping coefficient at the fundamental frequency of Model 1,2 and 3

Since the behavior of the frame was not measured without the upper bracing, it remains unknown what the contribution is of  $c_s$  and  $c_b$  to the total damping. Therefore, the exact damping coefficient of the auxiliary damping component in Figure 3.19A cannot be determined and the conclusion is only that the damping is indeed increased by 19.665Ns/m by the application of the auxiliary damping component including SBR5.

What other factors could have influenced the additional damping in the structure? The damping component in rest is displayed in Figure 3.19A. The layers of SBR are glued to the U-shaped aluminum profiles, which are connected to the bracing by bolts. Figure 3.19B displays the desired working principle of the damper: the layers of SBR were to be subjected to a shear force which would result in a shear strain of the SBR layers. In accordance with the literature review Chapter 5, the shear strain is related directly to the energy dissipation by the SBR layer. However, in practice, the working principle of the damper was different, see Figure 3.19C. In each test, the bolts were slightly released during the test by the application of the impact force on the structure. Therefore, the bracing was moved along the gap in the aluminum profile, which could have been an additional cause for damping since an additional friction force could have been introduced. Consequently, the shear strain in the SBR layers has been reduced as well and thus the energy dissipation by the dampers. The damping by friction could explain the higher damping coefficient caused by the auxiliary damping component. On the other hand, upon the release of the bolts, the stiffness of the bracing could have been reduced as well. This was not the case for Model 3, which showed the exact same fundamental frequency as Model 1.

Also, the layers of glue have not been taken into account. The layers were rubbery itself and may have caused some damping in the auxiliary damping component. However, this remains

unknown because no tests have been conducted on the connection of the layers of SBR to the aluminum profile.

The above analysis shows that the exact energy dissipation by the layers of SBR and correspondingly, its damping coefficient are still unknown. Many factors could have influenced the additional damping in Model 2. Hence, the layers of SBR cannot be studied in itself but the auxiliary damping component can. From the tests and above analysis it may be concluded that the damping component does indeed provides additional damping to the structural system but the exact energy dissipation by the individual parts remains unknown.

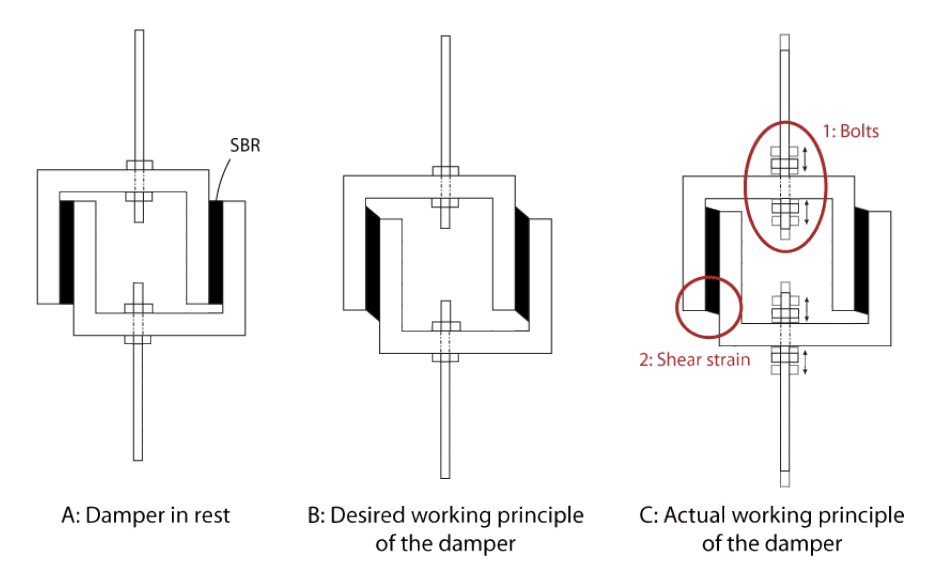


Figure 3.19: Auxiliary damping component in the bracing

## 3.5 Summary

In the above section the set-up and results from the physical test set-up were discussed. Two methods were employed to determine the damping ratio of the fundamental frequency of three different models and both methods showed similar results. However, a shift in frequency was measured for Model 2, which did not meet expectations. Further analysis of the structure of the FRFs implies the step size of the measured frequencies has been too big and thus the actual eigenfrequencies have not been measured accurately.

The peaks at higher frequencies in the FRF and the plot of the time signal imply a disturbed signal by higher frequencies. Therefore, higher frequencies could not be taken into account in further analysis of this test set-up.

Additionally, the relation between the layers of SBR and the test set-up has been studied and its influence on the overall behavior of the structure. It may be concluded the energy dissipation by the layers of SBR remains still unknown but additional damping is retrieved from the additional damping component which includes the SBR layers (Figure 3.19A). However, a 1-MSD model has been presented for future research to accurately determine the damping coefficient of the auxiliary damping component.

Also, an analysis has been conducted on factors that could possibly have influenced the damping in the structure. Connections, application of bracings and executional factors have been studied and each factor has a significant influence on the damping of the structure.

# 4 Vibrations in high rise structures

In this chapter, a mathematical model for a core structure and a braced portal frame structure will be presented.

## 4.1 Model set-up

In practice, high rise structures are often built as a combination of a core and (braced) portal frame structure. The basis of solving the NMSD system is the equation of motion:

$$Mu + C\dot{u} + Ku = F(t) \longleftrightarrow u + 2\zeta\omega_n\dot{u} + \omega_n^2 u = \frac{F(t)}{m_n}$$
 (4.1)

In Figure 4.1, the dynamical representation of a core structure is presented. The core structure is modeled as a flexural beam. Equivalently, each floor level in the structure is represented by a stiff element with elastic springs attached to it. The deformation of a single element causes a displacement in the vertical direction in each spring, see the red box in Figure 4.1. This displacement will be used in the next section to determine the stiffness matrix of the structure.

Since the along-wind direction is considered, it is convenient to find the stiffness of the structure in the x-direction, see Figure 4.1 (right). The stiffness matrix will be constructed from the relative displacement in the x-direction of each node. The relative displacement of node j is dependent on the displacement of nodes i, j and k.

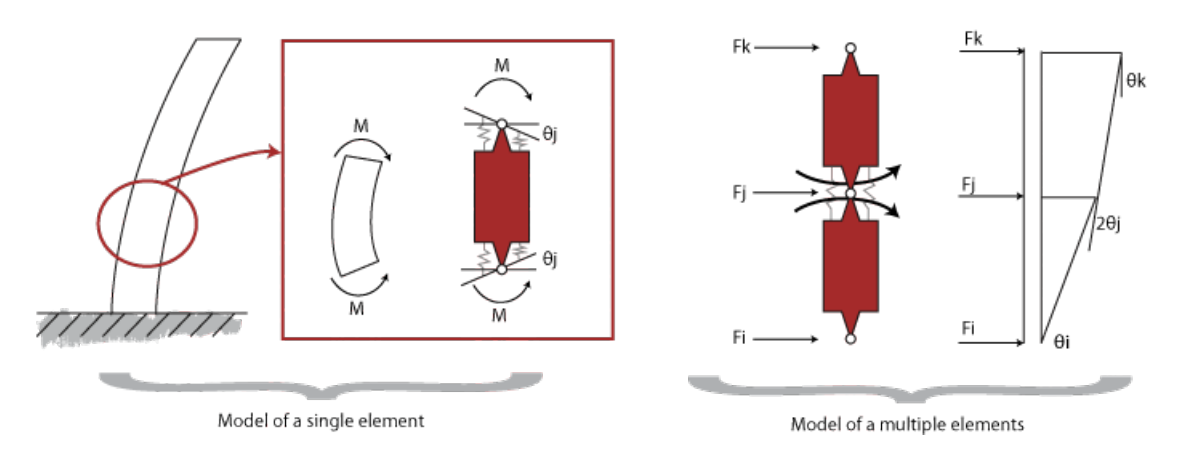


Figure 4.1: Stiffness of the core structure

The aim of the model is to determine the accelerations at the top of the building for a building with and without VEDs. These VEDs will be added to a braced portal frame structure. Beforehand, it is expected the application of VEDs will reduce the accelerations. The accelerations

will be calculated by the conduction of a spectral analysis; this method has been explained in Chapter 2.

The analysis will be executed for the 'Zalmhaven Toren', a 176 meter tall building which is supposed to be located in Rotterdam, see Figure 4.2.

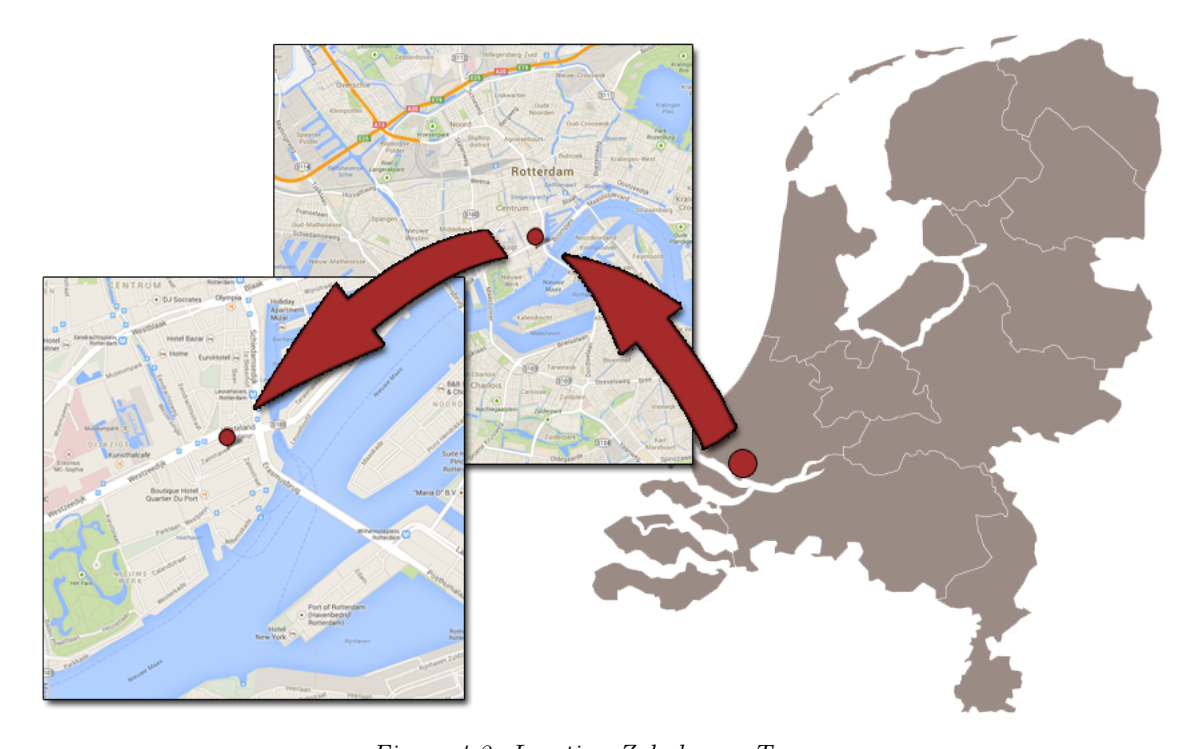


Figure 4.2: Location Zalmhaven Toren

The load bearing structure was designed to its final stage by Zonneveld Ingenieurs but the structure has not been built yet. An impression of the building is presented in Figure 4.3.



Figure 4.3: Impression Zalmhaven Toren

The structural properties were calculated and determined by Zonneveld Ingenieurs and are used as input parameters in the N-MSD model:  $^{[14]}$ 

• The load bearing structure consists of a concrete core with a flexural rigidity EI of 6.6185\*

4.1. MODEL SET-UP 35

 $10^{13} Nm^2$ .

• The dimensions are h = 176m, b = 30m and d = 30.8m. The dimensions of the concrete core are b = 10m and d = 10m. In reality, the height of the floor levels at the bottom and top of the is taller than the floor levels in between. However, for the model it is assumed the height of each floor level is the same, namely  $h_{storey} = 3.09$ m. This simplifies the model and it is expected the stiffness of the building will still be about the same in this situation.

- The total mass of the building is 70413000 kg. The mass is equally distributed over the 57 storeys and thus becomes:  $1.2353 * 10^6$  kg per storey.
- The rotational stiffness of the foundation is estimated to be  $8.52 * 10^{12} \ Nm/rad$ .
- The location of the building is in Rotterdam. This corresponds to terrain category IV and wind area 2 from NEN-EN 1991-1-4. Hence,  $z_0 = 1$ m,  $z_{min} = 10$ m and  $v_{b,0} = 27$ m/s.

### 4.1.1 Matrix definition

In this section, the definition of the matrices used for the equation of motion is presented. The scripts of the matrix definitions in Matlab is presented in Appendix G.

### Mass matrix

The mass matrix of a high rise structure with n floors is a diagonal matrix:

$$M = \begin{bmatrix} m_i & 0 & 0 & 0 \\ 0 & m_j & 0 & 0 \\ 0 & 0 & \ddots & 0 \\ 0 & 0 & 0 & m_N \end{bmatrix}$$

$$(4.2)$$

Where  $m_i$  is the mass of the  $i^{th}$  floor.

**Note:** an equal mass distribution per floor level is assumed with:  $m_i = m_{tot}/n$ .

#### Stiffness matrix

The stiffness matrix is constructed from a stiffness matrix of the core structure and the stiffness matrix of the foundation. The method to derive these matrices is presented in Appendix H.

#### Stiffness of the core structure

In accordance with Figure 4.1, the stiffness matrix of the j-th floor level in the core structure is determined by:<sup>[7]</sup>

$$k_{j,core} = \frac{EI}{h_{storey}^3} \begin{bmatrix} 1 & -2 & 1\\ -2 & 4 & 2\\ 1 & -2 & 1 \end{bmatrix}$$
 (4.3)

This element is implemented into the n \* n matrix in which n resembles the number of floors.

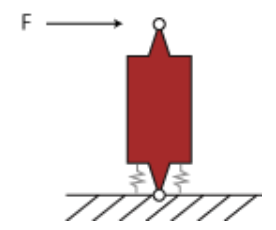


Figure 4.4: Bottom element of the core structure

#### Rotational stiffness of the foundation

The bottom element of the structure is modeled differently, see Figure 4.4. The rotational stiffness  $K_r$  of the foundation is estimated to be  $8.52*10^12 \ Nm/rad$ . The floor at ground level is modeled as:<sup>[7]</sup>

$$k_{foundation} = \frac{1}{l^2} \frac{1}{\frac{l}{2EI} + \frac{1}{K_c}} \begin{bmatrix} 1 & -1\\ -1 & 1 \end{bmatrix}$$
 (4.4)

This matrix will be added to the n \* n matrix at positions (1,1), (1,2), (2,1) and (2,2).

#### Corresponding stiffness matrix

The corresponding stiffness matrix of the entire structure is defined by:

$$K = K_{core} + k_{foundation} (4.5)$$

This matrix can be verified by adopting  $F = Ku \longrightarrow u = K^{-1}u$  in Matlab. The corresponding shape of the deformation is displayed in Figure 4.5. This is obtained by subjecting the structure to a distributed load of  $q = 100 \mathrm{kN/m}$ .

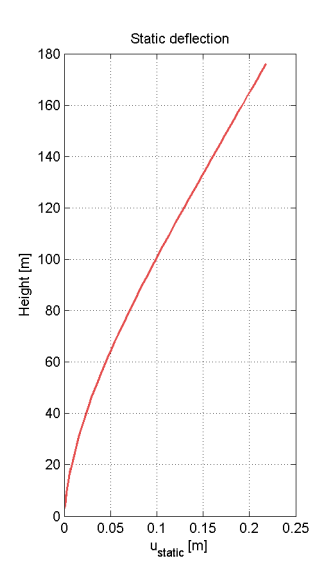


Figure 4.5: Static deflection of the structure

The result can be checked by hand by the use of a forget me not: [7;14]

$$u_{top} = u_{structure} + u_{foundation} = 1.2 * u_{structure} = 1.2 * \frac{qh^4}{8EI} = 1.2 * 0.18 = 0.22 m$$
 (4.6)

This corresponds to the displacement at the top in Figure 4.5 and thus the stiffness matrix is derived correctly.

4.1. MODEL SET-UP 37

#### 4.1.2 Damping matrix

The damping ratio or logarithmic decrement of the damping of each floor is obtained from:

$$\zeta = \zeta_s + \zeta_a + \zeta_d \quad ; \quad \delta = \delta_s + \delta_a + \delta_d \tag{4.7}$$

Respectively, this is the the structural, aerodynamic and auxiliary damping. The logarithmic decrement  $\delta$  and the damping ratio  $\zeta$  are related by  $\delta = \zeta 2\pi$ .

## Structural damping

The structural damping is obtained from Table F.2 from NEN-EN 1991-1-4 and is dependent on the applied material for the load bearing structure. In case of the Zalmhaven Toren, the structural damping is obtained from the concrete core. Hence, the logarithmic decrement of concrete  $\delta_s$  is 0.1 and its corresponding damping ratio  $\zeta_d$  becomes 0.016.

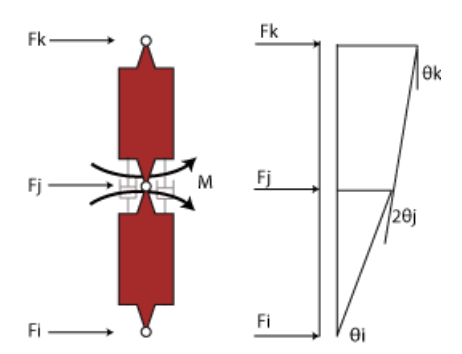


Figure 4.6: Structural damping in the core structure

The model for damping in the structure is displayed in Figure 4.6. Its corresponding damping matrix is constructed by adopting the Rayleigh damping method: [39]

$$C_{structure} = a_0 M + a_1 K (4.8)$$

Where  $a_0$  and  $a_1$  are constants depending on the first two eigenfrequencies and their corresponding damping ratios:

$$a_{0} = \frac{2\omega_{1}\omega_{2}(\zeta_{1}\omega_{2} - \zeta_{2}\omega_{1})}{\omega_{2}^{2} - \omega_{1}^{2}}$$

$$a_{1} = \frac{2(\zeta_{2}\omega_{2} - \zeta_{1}\omega_{1})}{\omega_{2}^{2} - \omega_{1}^{2}}$$
(4.9a)
$$(4.9b)$$

$$a_1 = \frac{2(\zeta_2 \omega_2 - \zeta_1 \omega_1)}{\omega_2^2 - \omega_1^2} \tag{4.9b}$$

In this case,  $\zeta_1 = \zeta_2 = 0.016$ .

## Aerodynamic damping

In accordance with NEN-EN 1991-1-4, the aerodynamic damping is to be found by:

$$\zeta_a = \frac{1}{2\pi} \frac{c_f \rho b v_m(z)}{2\omega_n m_e} \tag{4.10}$$

Hence, the aerodynamic damping varies along the height of the building.

**Note:** the aerodynamic damping will not be considered in this thesis

### 4.2 Model of the concrete core structure

In this section will be explained how the spectral analysis on the Zalmhaven Toren was conducted. First, a description will be presented on the model for the wind load on the structure. Secondly, the dynamic properties of the structure will be determined. Then, the response of the structure to the dynamic wind load will be studied. The influence on the response of the structure by adding SBR to the structure will be analyzed as well as the energy dissipation by the dampers. All Matlab scripts used for the calculations are to be found in Appendix G.

### 4.2.1 Wind load on the structure

The location of the building is Rotterdam. This corresponds to terrain category IV and wind area 2 from NEN-EN 1991-1-4. Hence,  $z_0 = 1$ m,  $z_{min} = 10$ m and  $v_{b,0} = 27$ m/s. The velocity of the wind consists of a mean and fluctuating part:

$$v_{tot} = \bar{v} + \tilde{v} \tag{4.11}$$

According to equation 4.3 in NEN-EN 1991-1-4 the mean wind speed along the height of the building of the wind may be described by: [29]

$$\bar{v}(z) = c_r(z)c_0(z)v_b 
= \begin{cases}
0.19v_b \left(\frac{z_0}{z_{0,II}}\right)^{0.07} ln\left(\frac{z_{min}}{z_0}\right) & z \le z_{min} \\
0.19v_b \left(\frac{z_0}{z_{0,II}}\right)^{0.07} ln\left(\frac{z}{z_0}\right) & z_{min} \le z \le z_{max}
\end{cases} (4.12)$$

The mean wind speed along the height of the Zalmhaven Toren is displayed in Figure 4.7. The fluctuating part of the velocity of the wind is to be determined stochastically. First, the standard deviation is determined in accordance with equation 4.6 of NEN-EN 1991-1-4:

$$\sigma_{v,wind} = k_r v_b k_l = 0.19 \left(\frac{z_0}{z_{0,II}}\right)^{0.07} v_b k_l = 0.19 \left(\frac{1}{0.005}\right)^{0.07} 27 * 1 = 7.4334 \quad [\text{m/s}] \quad (4.13)$$

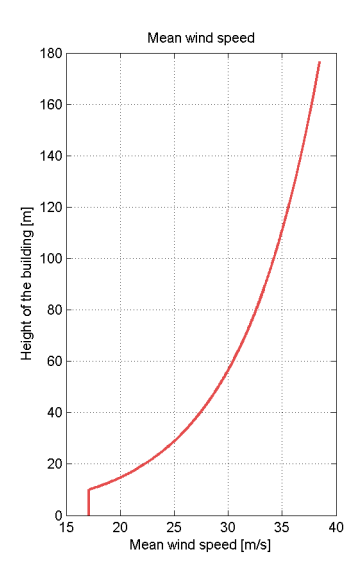


Figure 4.7: Wind speed along the height of the building

The fluctuating part of the wind speed is defined by: [43]

$$\tilde{v} = \sum_{k=1}^{N} a_k \sin(\omega_k t + \phi_k) \tag{4.14}$$

Where:

 $\begin{aligned} a_k &= \sqrt(2S_{vv,wind}\omega_k)\\ \phi_k &= \text{random number between 0 and } 2\pi \end{aligned}$ 

Hence, first the spectrum of the wind velocity is determined through:

$$S_{vv,wind} = \frac{\sigma_v^2 * F_D}{\omega} \tag{4.15}$$

The result is displayed in Figure 4.8 (top figure). In the above equation,  $F_D$  is Solari's spectrum and x is the dimensionless frequency described by: [43]

$$F_D = \frac{6.8x}{(1+10.2x)^{5/3}}$$

$$x = \frac{1}{2\pi} \frac{\omega L}{2\pi \bar{v}}$$

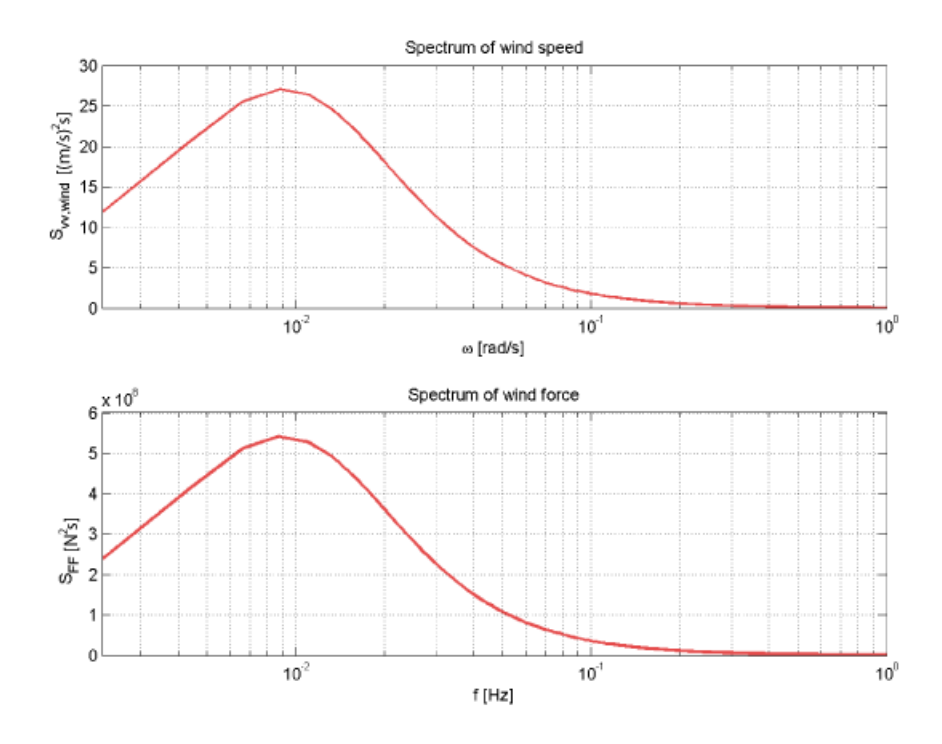


Figure 4.8: Spectrum of wind force

Combining Equations 4.14 and 4.15 leaves the fluctuating part of the wind velocity. Then, the spectrum of the wind load can be determined through:

$$S_{FF} = \chi^2 \left( C_p \rho_{air} \bar{v} A \right)^2 S_{vv,wind} \tag{4.16}$$

Where  $\chi^2$  is the aerodynamic admittance taking into account the coherence between different points at the façade of the structure. Full coherence is assumed and thus  $\chi^2 = 1$ . The spectrum of the wind force is displayed in Figure 4.8. With the load spectrum, the fluctuating wind force can be determined through:

$$F_w = \sum_{k=1}^{N} a_k \sin(\omega_k t + \phi_k) \tag{4.17}$$

Where:

 $\begin{array}{l} a_k = \sqrt(2S_{FF}\omega_k) \\ \phi_k = {\rm random~number~between~0~and~} 2\pi \end{array}$ 

The velocity and wind load on the façade are displayed in Figure 4.9.

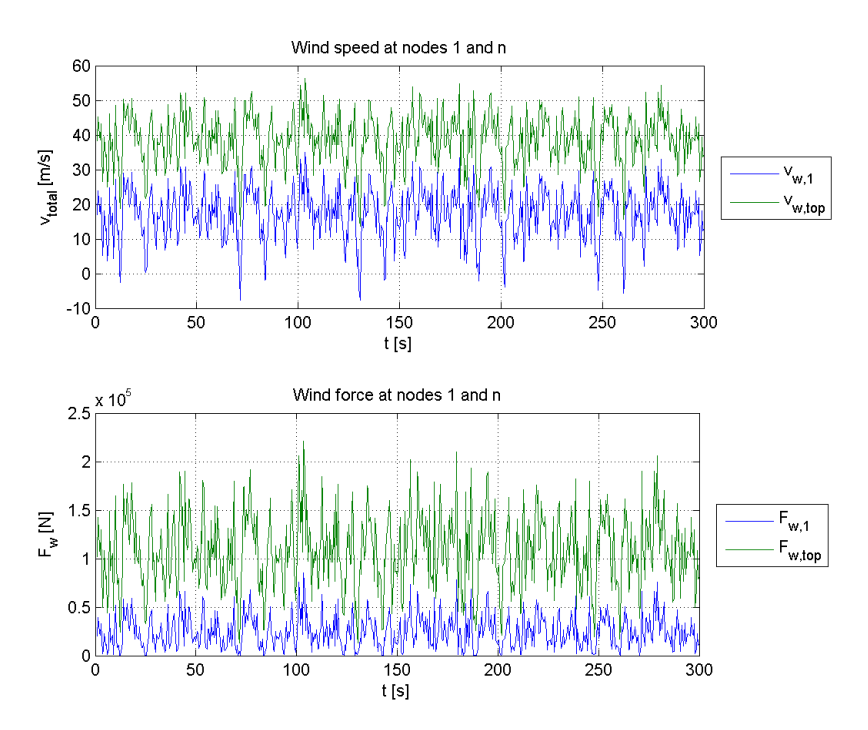


Figure 4.9: Wind speed including mean and fluctuating part

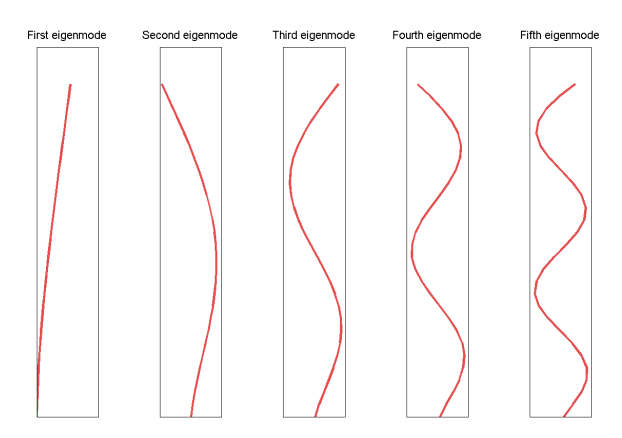


Figure 4.10: First five eigenmodes of the high rise structure

## 4.2.2 The structure's sensitivity to vibrations

The properties of the structures are resembled by its corresponding M, K and C matrices. The eigenfrequencies of the structure are found from the eigenvalues of the M and K matrix. Its corresponding eigenvectors could be used to check if this is done correctly by finding the eigenmodes of the structure. Hence, the first five eigenmodes of the modeled building are displayed in Figure 4.10.

The shapes displayed in this figure are legitimate and thus the eigenfrequencies are calculated correctly.

The M, K and C matrices could be used to determine the frequency dependent dynamic stiffness  $S_u$  of the system. The dynamic stiffness coefficient may be used to find the transfer function  $H_u$  through the following relation:

$$S_u = K - \omega^2 M + i\omega C \quad \longleftrightarrow \quad H_u = \left\{ K - \omega^2 M + i\omega C \right\}^{-1} \tag{4.18}$$

As was described in Chapter 2, respectively the displacement, velocity and acceleration of a system are described by: [26]

$$u = |H_{uF}|F$$
 ;  $v = |H_{vF}|F = |\omega H_{uF}|F$  ;  $a = |H_{aF}|F = |\omega^2 H_{uF}|F$  (4.19)

Then, the transfer functions at the top of the building are described by: [7]

$$|H_{uF,N}(\omega)| = \sum_{j=1}^{N} |H_{uFj,N}|$$
 (4.20a)

$$|H_{vF,N}(\omega)| = \sum_{j=1}^{N} |H_{vFj,N}|$$
 (4.20b)

$$|H_{aF,N}(\omega)| = \sum_{j=1}^{N} |H_{aFj,N}|$$
 (4.20c)

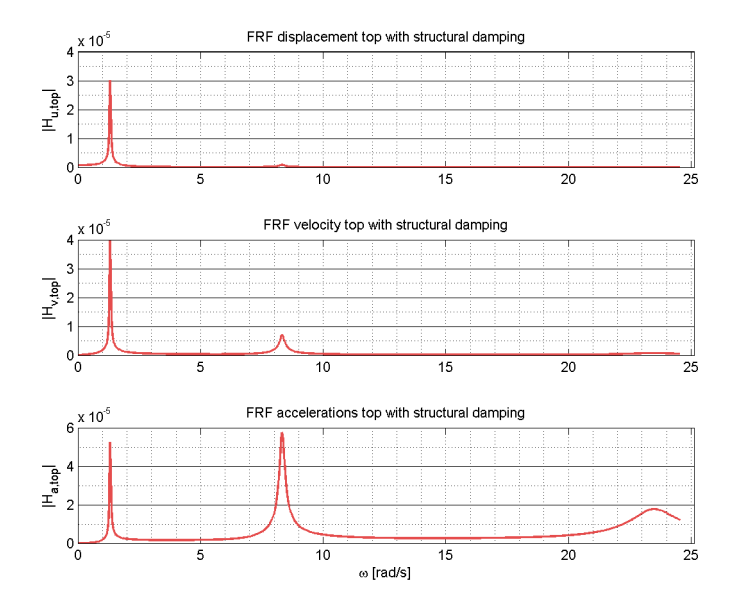


Figure 4.11: Frequency response function of the structure without VED

The result for the Zalmhaven Toren without SBR dampers is displayed in Figure 4.11. The fundamental frequency is about 1.3 rad/s, which corresponds to  $f_0 = 0.223$ Hz. The fundamental frequency calculated by Zonneveld Ingenierus is 0.286Hz. The results differ because the N-MSD model was assumed to have an equal storey height for each floor level while the height of the storeys in the model of Zonneveld Ingenieurs differed. [14]

## 4.2.3 Response of the structure

The response spectra of the displacement, velocity and acceleration are obtained by: [43]

$$S_{uu} = |H_{uF,N}(\omega)|^2 S_{FF} \tag{4.21a}$$

$$S_{vv} = |H_{vF,N}(\omega)|^2 S_{FF} \tag{4.21b}$$

$$S_{aa} = |H_{aF,N}(\omega)|^2 S_{FF} \tag{4.21c}$$

The spectra of the Zalmhaven Toren without SBR dampers is displayed in Figure 3.13.

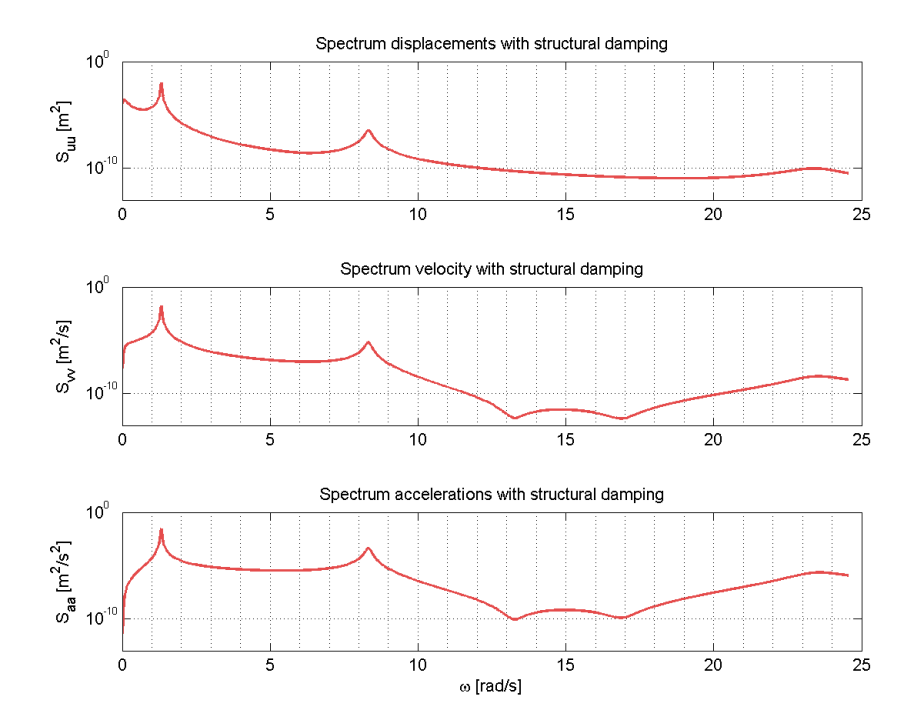


Figure 4.12: Spectra of displacement, velocity and accelerations of the structure without VED

The response over time of the displacement, velocity and acceleration of the Zalmhaven Toren is obtained from the above spectrum by finding its Fourier transform. Hence, the same procedure is used as for the wind velocity (Equation 4.14) and wind force (Equation 2.2). The result is displayed in Figure 4.13.

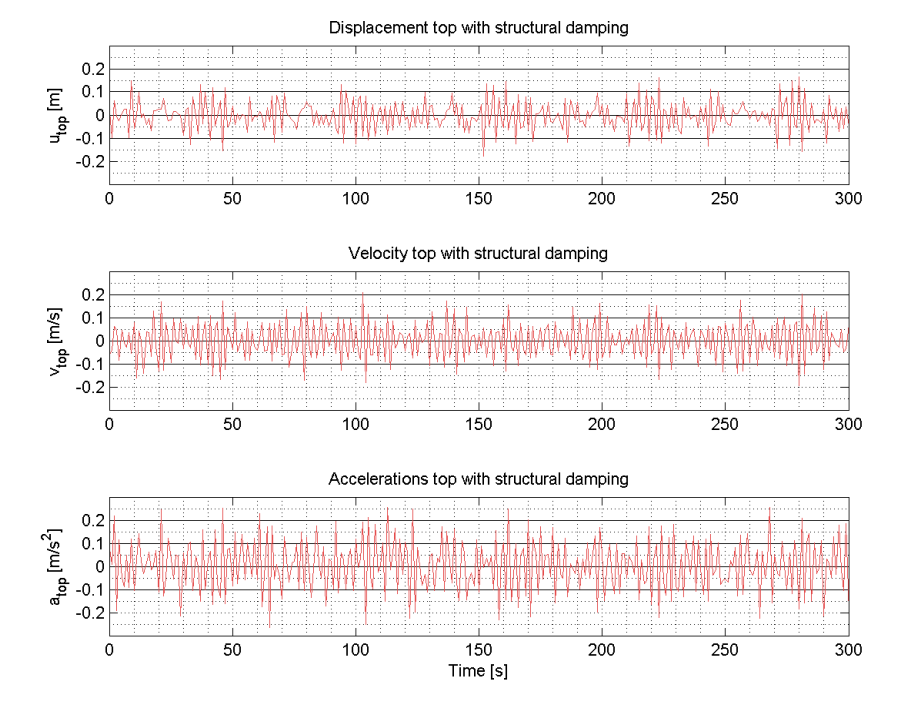


Figure 4.13: Response of the structure without VED of the displacement, velocity and accelerations

The spectra in Figure 4.12 are used to find the standard deviations of the responses:

$$\sigma_u = \sqrt{\int_0^\infty S_{uu}(\omega)d\omega}$$
 (4.22a)

$$\sigma_v = \sqrt{\int_0^\infty S_{vv}(\omega) d\omega}$$
 (4.22b)

$$\sigma_a = \sqrt{\int_0^\infty S_{aa}(\omega)d\omega} \tag{4.22c}$$

The corresponding values are presented in Table 4.1. The peak values in this table have been calculated by multiplying the standard deviations by the peak factor  $k_p$  from equation B.4 of NEN-EN 1991-1-4:

$$k_p = \sqrt{2\ln(vT)} + \frac{0.6}{\sqrt{2\ln(vT)}}$$
 (4.23)

With T = 600s and v = 0.223Hz,  $k_p = 3.3$ . The peak values obtained from this method cover most of the peaks displayed in Figure 4.13. However, the highest peaks are higher in the figure than the values in Table 4.1.

Table 4.1: Standard deviations of displacement, velocity and accelerations and the peak accelerations for the structure with and without SBR3 and SBR5

Type	$\sigma_u[\mathrm{m}]$	$\sigma_v[{ m m/s}]$	$\sigma_a[{\rm m/s^2}]$	$u_{peak}[\mathrm{m}]$	$v_{peak}[\mathrm{m/s}]$	$a_{peak}[\mathrm{m/s^2}]$
$c_s$	0.0236	0.0292	0.0402	0.078	0.096	0.133

## 4.3 A basis for a model of a portal frame structure

In this section a mathematical description will be presented for the elements in a single portal frame structure to determine the dynamical behavior with and without damping.

This description is the basis for a model of stacked portal frames in a high rise structure.

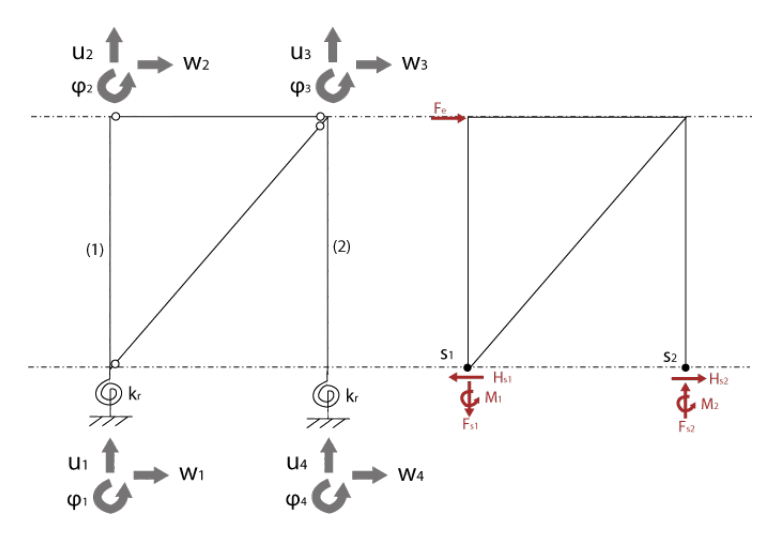


Figure 4.14: Model of the portal frame structure and degrees of freedom (left) and support reactions (right)

### 4.3.1 Definition of the elements

A single undamped braced portal frame structure consists of five elements, see Figure 4.14. In correspondence with the physical test set-up, the structure is loaded at the top by a point load  $F_e$ . The force is transferred to the foundation to two supports. The corresponding balance of forces in the nodes is presented in Figure 4.15.

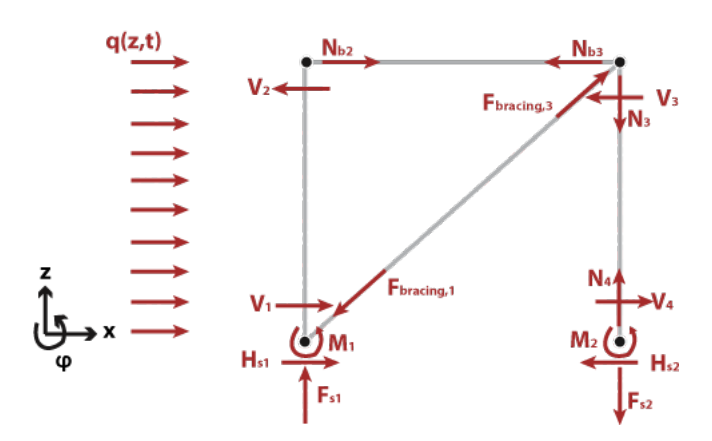


Figure 4.15: Balance of forces in each node

The columns of the portal frame structure are bending beams. Additionally, the columns are axially loaded. The model of the columns is presented in Figure 4.16. The columns are assumed to be prismatic and both to have the same cross-sectional area and material properties.

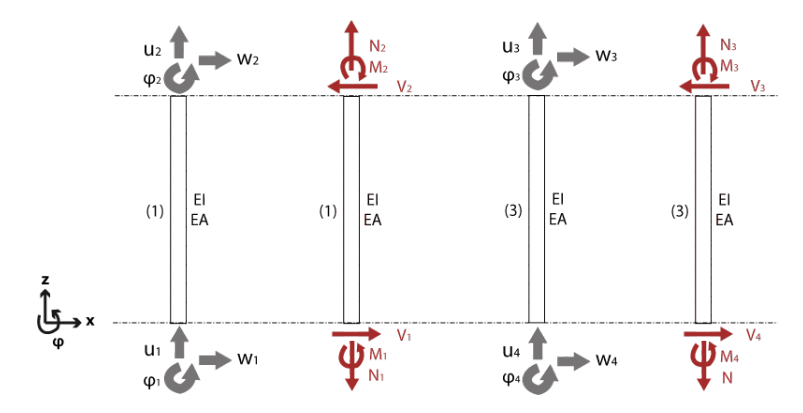


Figure 4.16: Model of the columns of the portal frame structure

## 4.3.2 Dynamic stiffness matrices of the elements

In this section the dynamic stiffness matrix for each element will be derived.

## Bending beam

In accordance with the Euler-Bernoulli beam theory the equation of motion for the bending beam is described by:

$$EI\frac{\partial^4 w}{\partial z^4} + E^*I\frac{\partial^5 w}{\partial t \partial z^4} + \rho A\frac{\partial^2 w}{\partial t^2} = q(z, t)$$
(4.24)

The above equation may be transformed to the frequency domain by the application of the Fourier transform:

$$\int_{-\infty}^{\infty} \left[ EI \frac{\partial^4 w}{\partial z^4} + E^* I \frac{\partial^5 w}{\partial t \partial z^4} + \rho A \frac{\partial^2 w}{\partial t^2} \right] e^{-i\omega t} dt = \int_{-\infty}^{\infty} q(z, t) e^{-i\omega t} dt$$
 (4.25)

Then, the displacement w becomes:

$$W = \int_{-\infty}^{\infty} w e^{-i\omega t} dt \tag{4.26}$$

Correspondingly, the governing homogeneous equation in the frequency domain becomes:

$$\hat{W}^{""} - \beta^4 \hat{W} = 0 \quad \text{with} \quad \beta^4 = \frac{\rho A \omega^2}{EI + i\omega E^* I}$$

$$\tag{4.27}$$

Correspondingly, the roots of the equation will become:

$$r^2 = \beta^2$$
 with  $\beta^4 = \frac{\rho A \omega^2}{EI + i\omega E^* I}$  and  $r_{b2} = -r_{b1}$  ;  $r_{b4} = -r_{b3}$  (4.28)

The homogeneous solution is expressed by: [26;35]

$$W_{hom}(x,\omega) = C_1 \cosh(\beta z) + C_2 \sinh(\beta z) + C_3 \cos(\beta z) + C_4 \sin(\beta z)$$

$$\tag{4.29}$$

Where  $C_1$  to  $C_4$  are integration constants to be determined from the boundary conditions. The governing equation to find the particular solution is expressed by:

$$\hat{W}^{""} - \beta^4 \hat{W} = \frac{Q(z, \omega)}{EI + i\omega E^* I} \quad \text{with} \quad \beta^4 = \frac{\rho A \omega^2}{EI + i\omega E^* I}$$

$$(4.30)$$

In accordance with NEN-EN 1991-1-4, the load is expressed by:

$$Q(z,\omega) = Q_0(\omega) \ln\left(\frac{z}{z_0}\right) = Q_0 \left(B_1 + B_2 e^{-z/B_3}\right)$$
(4.31)

Where  $B_1$ ,  $B_2$  and  $B_3$  are coefficients to approach the logarithmic function by means of the exponential function. This simplifies the method to define the particular solution. The particular solution will be in the same form as the load on the structure. Therefore, the form of the particular solution is:<sup>[3]</sup>

$$W_{part}(z,\omega) = C_0(\omega) + C_z(\omega)e^{-z/B_3}$$
(4.32)

And thus:

$$-\beta^{4}C_{0} + \left[ \left( -\frac{1}{B_{3}} \right)^{4} - \beta^{4} \right] C_{z} e^{-z/B_{3}} = \frac{Q_{0} \left( B_{1} + B_{2} e^{-z/B_{3}} \right)}{EI + i\omega E^{*}I} = \frac{Q_{0}B_{1}}{EI + i\omega E^{*}I} + \frac{Q_{0}B_{2} e^{-z/B_{3}}}{EI + i\omega E^{*}I}$$

$$(4.33)$$

In correspondence with Equation 4.32 the constants in the particular solution are: [3]

$$C_0(\omega) = \frac{-B_1 Q_0(\omega)}{\beta^4 (EI + i\omega E^*I)} \quad ; \quad C_z(\omega) = \frac{-B_2 Q_0(\omega)}{EI + i\omega E^*I} \frac{1}{\left(-\frac{1}{B_3}\right)^4 - \beta^4}$$
(4.34)

The general solution to the system is the summation of the homogeneous and particular solution:

$$W(z,\omega) = W_{hom}(z,\omega) + W_{part}(z,\omega)$$

$$= C_1 \cosh(\beta z) + C_2 \sinh(\beta z) + C_3 \cos(\beta z) + C_4 \sin(\beta z) + C_0(\omega)$$

$$+ C_z(\omega) e^{-z/B_3}$$
(4.35)

The inverse Fourier Transform can be used to find the particular solution in the time domain:

$$w(z,t) = \frac{1}{2\pi} \int_{-\infty}^{\infty} W(z,\omega) e^{i\omega t} d\omega$$
 (4.36)

The coefficients  $C_1$ ,  $C_2$ ,  $C_3$  and  $C_4$  can be determined from the boundary conditions of the specific element. This will be done in the next section.

#### Element 1

The boundary conditions in the frequency domain for Element 1:

1. 
$$z = 0$$
;  $(EI + i\omega E^*I)W'' = k_rW'$ 

2. 
$$z = 0$$
;  $(EI + i\omega E^*I)W''' = \int_{-\infty}^{\infty} [-H_{s1}(t) + F_{bracing,x1}(t)] e^{-i\omega t} dt$ 

3. 
$$z = h$$
;  $(EI + i\omega E^*I)W'' = 0$ 

4. 
$$z = h$$
;  $(EI + i\omega E^*I)W''' = \int_{-\infty}^{\infty} N_{b2}(t)e^{-i\omega t}dt$ 

Implementation of the general solution into the above boundary conditions leaves:

$$\beta^{2}(EI + i\omega E^{*}I) \left[C_{1} - C_{3}\right] - k_{r}\beta \left[C_{2} + C_{4}\right] = F_{1,1}$$
(4.37a)

$$\beta^{3}(EI + i\omega E^{*}I) \left[C_{2} - C_{4}\right] = F_{1,2} \tag{4.37b}$$

$$\beta^{2}(EI + i\omega E^{*}I)\left[C_{1}\cosh(\beta h) + C_{2}\sinh(\beta h) - C_{3}\cos(\beta h) - C_{4}\sin(\beta h)\right] = F_{1,3}$$
 (4.37c)

$$\beta^{3}(EI + i\omega E^{*}I)\left[C_{1}\sinh(\beta h) + C_{2}\cosh(\beta h) + C_{3}\sin(\beta h) - C_{4}\cos(\beta h)\right] = F_{1,4}$$
 (4.37d)

With Element 1 subjected to the load  $Q(z,\omega)$ , the loads in the above equation are expressed by:

$$F_{1,1} = -\left[\frac{k_r}{B_3} + \frac{(EI + i\omega E^*I)}{B_3^2}\right] C_z(\omega)$$
 (4.38a)

$$F_{1,2} = \int_{-\infty}^{\infty} H_{s1}(t)e^{-\mathrm{i}\omega t}dt + \int_{-\infty}^{\infty} F_{bracing,x1}(t)e^{-\mathrm{i}\omega t}dt + \left[\frac{(EI + i\omega E^*I)}{B_3^3}\right]C_z(\omega)$$
 (4.38b)

$$F_{1,3} = -\left[\frac{(EI + i\omega E^*I)}{B_3^2}e^{-h/B_3}\right]C_z(\omega)$$
(4.38c)

$$F_{1,4} = \int_{-\infty}^{\infty} F_{k_{b2}}(t)e^{-i\omega t}dt + \left[\frac{(EI + i\omega E^*I)}{B_3^3}e^{-h/B_3}\right]C_z(\omega)$$
(4.38d)

The above in matrix notation

$$\beta^{2}(EI + i\omega E^{*}I) \begin{bmatrix} 1 & -\frac{k_{r}}{\beta(EI + i\omega E^{*}I)} & -1 & -\frac{k_{r}}{\beta(EI + i\omega E^{*}I)} \\ 0 & \beta & 0 & -\beta \\ \cosh(\beta h) & \sinh(\beta h) & -\cos(\beta h) & -\sin(\beta h) \\ \beta \sinh(\beta h) & \beta \cosh(\beta h) & \beta \sin(\beta h) & -\beta \cos(\beta h) \end{bmatrix} \begin{bmatrix} C_{1} \\ C_{2} \\ C_{3} \\ C_{4} \end{bmatrix} = \begin{bmatrix} F_{1,1} \\ F_{1,2} \\ F_{1,3} \\ F_{1,4} \end{bmatrix}$$
(4.39)

Hence, the coefficients  $C_1$ ,  $C_2$ ,  $C_3$  and  $C_4$  could now be determined and then be implemented into the general solution.

#### Element 2

The boundary conditions in the frequency domain for Element 2:

1. 
$$z = 0$$
;  $(EI + i\omega E^*I)W'' = k_rW'$ 

2. 
$$z = 0$$
;  $(EI + i\omega E^*I)W''' = \int_{-\infty}^{\infty} H_{s2}(t)e^{-i\omega t}dt$ 

3. 
$$z = h$$
:  $(EI + i\omega E^*I)W'' = 0$ 

4. 
$$z = h$$
;  $(EI + i\omega E^*I)W''' = \int_{-\infty}^{\infty} [F_{bracing,x3}(t) - N_{b3}(t)] e^{-i\omega t} dt$ 

Implementation of the general solution into the above boundary conditions leaves:

$$\beta^{2}(EI + i\omega E^{*}I) \left[C_{5} - C_{7}\right] - k_{r}\beta \left[C_{6} + C_{8}\right] = F_{2.1}$$
(4.40a)

$$\beta^{3}(EI + i\omega E^{*}I) [C_{6} - C_{8}] = F_{2,2}$$
(4.40b)

$$\beta^{2}(EI + i\omega E^{*}I)\left[C_{5}\cosh(\beta h) + C_{6}\sinh(\beta h) - C_{7}\cos(\beta h) - C_{8}\sin(\beta h)\right] = F_{2,3}$$
 (4.40c)

$$\beta^{3}(EI + i\omega E^{*}I)\left[C_{5}\sinh(\beta h) + C_{6}\cosh(\beta h) + C_{7}\sin(\beta h) - C_{8}\cos(\beta h)\right] = F_{2,4}$$
 (4.40d)

Element 2 is not being subjected to an external load and thus the loads in the above equation are expressed by:

$$F_{2,1} = 0 (4.41a)$$

$$F_{2,2} = \int_{-\infty}^{\infty} H_{s2}(t)e^{-\mathrm{i}\omega t}dt \tag{4.41b}$$

$$F_{2,3} = 0$$
 (4.41c)

$$F_{2,4} = \int_{-\infty}^{\infty} \left[ F_{bracing,x3}(t) - F_{k_{b3}}(t) \right] e^{-i\omega t} dt \tag{4.41d}$$

The above in matrix notation:

$$\beta^{2}(EI + i\omega E^{*}I) \begin{bmatrix} 1 & -\frac{k_{r}}{\beta(EI + i\omega E^{*}I)} & -1 & -\frac{k_{r}}{\beta(EI + i\omega E^{*}I)} \\ 0 & \beta & 0 & -\beta \\ \cosh(\beta h) & \sinh(\beta h) & -\cos(\beta h) & -\sin(\beta h) \\ \beta \sinh(\beta h) & \beta \cosh(\beta h) & \beta \sin(\beta h) & -\beta \cos(\beta h) \end{bmatrix} \begin{bmatrix} C_{5} \\ C_{6} \\ C_{7} \\ C_{8} \end{bmatrix} = \begin{bmatrix} F_{2,1} \\ F_{2,2} \\ F_{2,3} \\ F_{2,4} \end{bmatrix}$$
(4.42)

Thus, the coefficients  $C_5$ ,  $C_6$ ,  $C_7$  and  $C_8$  could now be determined and then be implemented into the general solution.

## Axially loaded beam

The general equation to describe the motion for the axially loaded beam is described by: [26]

$$EA\frac{\partial^2 u}{\partial x^2} + E^*A\frac{\partial^3 u}{\partial t \partial x^2} + \rho A\frac{\partial^2 u}{\partial t^2} = q(z, t)$$
(4.43)

Where  $c_s$  is the structural damping of the element. The governing differential equation in the frequency domain becomes: [46]

$$\hat{U}'' + \frac{\omega^2 \rho A}{EA + i\omega E^* A} \hat{U} = 0 \tag{4.44}$$

The corresponding characteristic equation and its roots is expressed by:

$$r^2 + a^2 = 0 \quad \longleftrightarrow \quad r_{1,2} = \pm \sqrt{\frac{\omega^2 \rho A}{EA + i\omega E^* A}}$$

$$\tag{4.45}$$

The homogeneous solution is described by: [26;35]

$$U_{hom}(z,\omega) = A_1 \cos(az) + A_2 \sin(az) \quad \text{where:} \quad a = \sqrt{\frac{\omega^2 \rho A}{EA + i\omega E^* A}}$$
 (4.46)

The governing equation for the particular solution becomes:

$$\hat{U}'' + \frac{\omega^2 \rho A}{EA + i\omega E^* A} \hat{U} = \frac{Q(x, \omega)}{EI + i\omega E^* A} \tag{4.47}$$

The load q(z,t) = 0 and thus the general solution equals the homogeneous solution. Therefore, the above equation will not be considered further.

#### Element 1

The boundary conditions in the frequency domain for Element 1:

1. 
$$z = 0$$
;  $(EA + i\omega E^*A)U' = 0$ 

2. 
$$z = h$$
;  $(EA + i\omega E^*A)U' = 0$ 

Implementation of the general solution into the above boundary conditions leaves:

$$a(EA + i\omega E^*A)A_2 = N_1 = 0 (4.48a)$$

$$a(EA + i\omega E^*A) [-A_1 \sin(ah) + A_2 \cos(ah)] = N_2 = 0$$
(4.48b)

And thus:

$$a(EA + i\omega E^*A) \begin{bmatrix} 0 & 1 \\ -\sin(ah) & \cos(ah) \end{bmatrix} \begin{bmatrix} A_1 \\ A_2 \end{bmatrix} = \begin{bmatrix} N_1 \\ N_2 \end{bmatrix}$$
(4.49)

#### Element 3

The boundary conditions in the frequency domain for Element 2:

1. 
$$z = 0$$
;  $(EA + i\omega E^*A)U' = \int_{-\infty}^{\infty} F_{s2}e^{-i\omega t}dt$ 

2. 
$$z = h$$
;  $(EA + i\omega E^*A)U' = \int_{-\infty}^{\infty} F_{bracing,z3}e^{-i\omega t}dt$ 

Implementation of the general solution into the above boundary conditions leaves:

$$a(EA + i\omega E^*A)A_4 = N_4 = \int_{-\infty}^{\infty} F_{s2}(t)e^{-i\omega t}dt$$
 (4.50a)

$$a(EA + i\omega E^*A)\left[-A_3\sin(ah) + A_4\cos(ah)\right] = N_3 = \int_{-\infty}^{\infty} F_{bracing,z3}(t)e^{-i\omega t}dt$$
 (4.50b)

And thus:

$$a(EA + i\omega E^*A) \begin{bmatrix} 0 & 1\\ -\sin(ah) & \cos(ah) \end{bmatrix} \begin{bmatrix} A_3\\ A_4 \end{bmatrix} = \begin{bmatrix} N_3\\ N_4 \end{bmatrix}$$
(4.51)

## Model of the beam and bracing

The stiffness of the beam  $k_b$  is presented by  $\frac{EA}{l_b}$ , where  $l_b$  is the length of the beam

$$\begin{bmatrix} F_{k_{b2}} \\ F_{k_{b3}} \end{bmatrix} = \frac{EA}{l_b} \begin{bmatrix} 1 & -1 \\ -1 & 1 \end{bmatrix} \begin{bmatrix} w_2 \\ w_3 \end{bmatrix}$$
(4.52)

The stiffness  $k_s$  of the bracing is presented by  $\frac{EA}{l_s}$ , where l is the length of the bracing. Hence, for the undamped case presented in Figure 4.17A,  $F_{bracing,1}$  is resembled by  $k_s(w_1' - w_3')$ , where  $w_1'$  and  $w_3'$  are the displacements in the direction of the bracing. Correspondingly, the force from the bracing in the undamped case can be rewritten as:

$$\begin{bmatrix} F_{bracing,1} \\ F_{bracing,3} \end{bmatrix} = \frac{EA}{l_s} \begin{bmatrix} 1 & -1 \\ -1 & 1 \end{bmatrix} \begin{bmatrix} w_1' \\ w_3' \end{bmatrix}$$

$$(4.53)$$

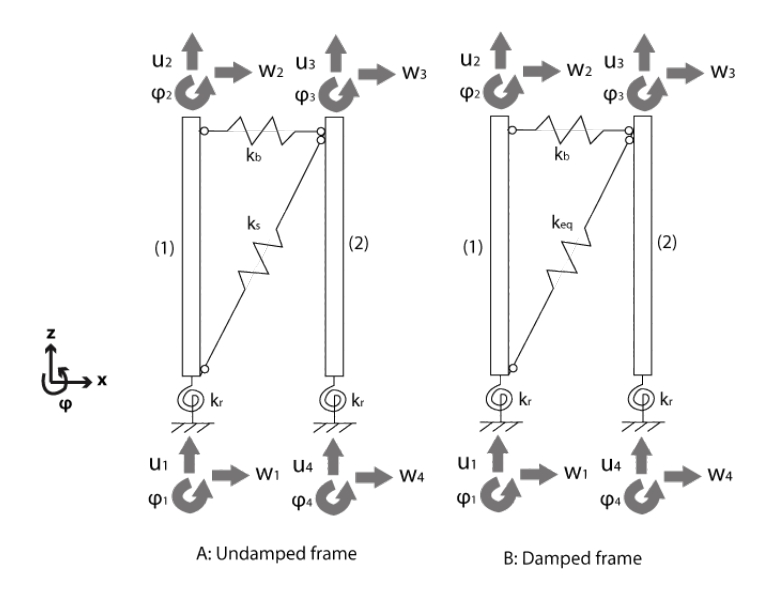


Figure 4.17: Dynamic model of a portal frame structure

In Figure 4.17B the VED is added to the bracing. In this case, the equation of the force from the bracing transferred to the two columns becomes more difficult and an equivalent spring stiffness

is introduced, which includes the spring and damper elements in the bracing. Accordingly, the equation for the bracing is described by:

$$\begin{bmatrix} F_{bracing,1} \\ F_{bracing,3} \end{bmatrix} = k_{eq} \begin{bmatrix} 1 & -1 \\ -1 & 1 \end{bmatrix} \begin{bmatrix} w_1' \\ w_3' \end{bmatrix}$$
(4.54)

Where  $k_{\parallel}eq$  is dependent on the layout of the bracing. An example has been presented in Chapter 3, where a formula was presented for the equivalent damping of the bracing in the test set-up.

In all the above equation the force in the direction of the bracing can be split up in its equivalent horizontal and vertical part:

$$\begin{bmatrix}
F_{bracing,x1} \\
F_{bracing,x3}
\end{bmatrix} = \cos(\alpha) \begin{bmatrix}
F_{bracing,1} \\
F_{bracing,3}
\end{bmatrix}$$

$$\begin{bmatrix}
F_{bracing,z1} \\
F_{bracing,z3}
\end{bmatrix} = \sin(\alpha) \begin{bmatrix}
F_{bracing,1} \\
F_{bracing,3}
\end{bmatrix}$$
(4.55a)

$$\begin{bmatrix}
F_{bracing,z1} \\
F_{bracing,z3}
\end{bmatrix} = \sin(\alpha) \begin{bmatrix}
F_{bracing,1} \\
F_{bracing,3}
\end{bmatrix}$$
(4.55b)

#### 4.3.3 Conclusion

The above descriptions of the bending beams and connected bracings can be used to determine the behavior of a single portal frame structure. A system of eight equations and unknowns has been derived for the bending beam and a system of two equations and two unknowns for the axially loaded beam. Additionally, a method has been presented to connect the two beams through additional elements, namely a horizontally positioned beam and a bracing.

#### 4.4 The prototype tool

The interface of the prototype tool is displayed in Figure 4.18.

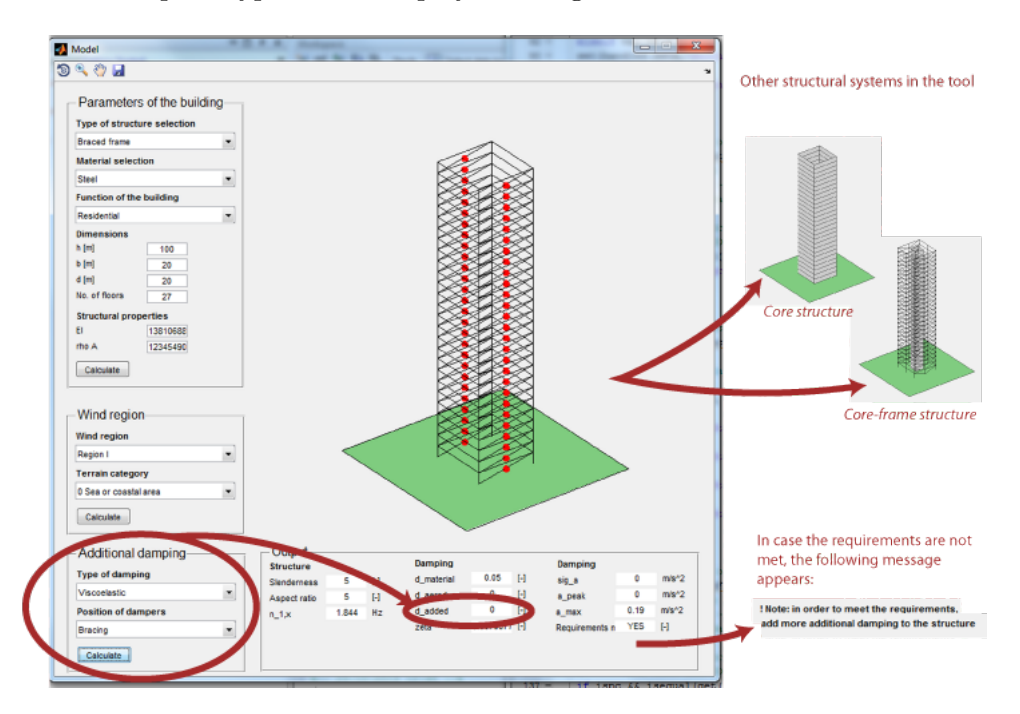


Figure 4.18: Interface of the prototype tool

Within the tool, four sections can be distinguished:

- 1. **Parameters of the building:** the structural designer can make a selection from types of structures, materials and the function of the building. Additionally, it allows the user to define structural parameters such as dimensions, the bending stiffness and the mass of the structure. After running the calculations, a visual presentation of the structure appears
- 2. Wind region: selections can be made regarding the wind region of the building in accordance with NEN-EN 1991-1-4
- 3. Additional damping: allows the structural designer to define specifications of the auxiliary damping system. The position of the damper is presented visually in the image
- 4. **Output:** this section provides the output of the calculations performed with the above input. Structural parameters such as the stiffness and slenderness are calculated along with the total logarithmic decrement of the structure and auxiliary dampers. Also, the peak accelerations are calculated as well as the maximum allowed acceleration. In case the requirements are not met, a warning will appear at the bottom of the interface which recommends the user to add more damping to the structure.

In future research, this could be the starting point of the actual development of the tool.

# 5 Conclusions

In this chapter the conclusions with regards to the research will be presented. The main objective for this thesis has been:

A feasibility study on the development of a prototype tool for engineering firms which can be used to determine the required amount of viscoelastic damping in a high rise structure to reduce accelerations to a comfortable level'

First, conclusions will be drawn for the two conducted investigations described in Chapter 3 and 4. Then, the final conclusion will be a discussion on the above objective. Next, expectations will be presented on how the obtained results will be applicable to related topics. Finally, recommendations will be presented for future research. A summary of this chapter is to be found in the next chapter.

#### 5.1 Conclusions

As was presented in Chapter 3, the thesis has been divided into the following two investigations:

- 1. Investigation on VED by means of a physical test set-up
- 2. Investigation on modeling a NMSD as a basis for the prototype tool

The conclusions drawn from these investigations are presented below. Then, the results will be adopted into a general conclusion on the main aim of research.

## 5.1.1 Conclusions from the physical test set-up

A braced portal frame structure has been used to determine the effect of the application of a damping component on the behavior of the structure. Measurements were taken in the frequency domain with step size  $\Delta f = 0.067 \mathrm{Hz}$  and in the time domain with step size  $\Delta t = 0.001 \mathrm{s}$ . The damping ratio of the structure with and without the auxiliary damping component has been determined in two ways:

- From the FRF through the half-power bandwidth method
- From the time signal through the logarithmic decrement

The obtained values from both methods were compared to one another and were approximately the same. The structure has been changed slightly several times:

- Removal of the upper and lower bracing
- Changes in the connection of the beams to columns

5.1. CONCLUSIONS 53

• Introduction of an auxiliary damping component with layers of VEM of 3 mm and 5 mm thick

From these changes it may be concluded that the global damping of the structure can be increased by many factors:

- Damping by friction
- Material damping
- Factors within the damping component:
  - Damping by friction
  - Material damping
  - Damping by adhesive layer (glue)
  - Layers of viscoelastic material

Hence, if a higher damping coefficient is required to reduce accelerations, each of these factors may be changed. However, it is expected the introduction of a damping component is most efficient. Additionally, adding damping through a damping component does not require tremendous changes in the structural system.

Now, if the factors in the damping component are studied into more detail, it becomes clear that the amount of energy dissipation by each single factor remains still unknown because the model for the bracing becomes rather complex, see Figure 3.10. The only certainty is that the component as a whole dissipates energy from the structural system and reduces the accelerations. This results in a list of known unknowns:

- What is the amount of energy dissipated by each single factor?
- What causes energy dissipation by each single factor?
- Is it possible to optimize the damper to obtain a higher energy dissipation?

These questions can be used as starting points for future research. The literature review can be used as a starting point to answer these questions. For example, in the literature review has been presented that the damping coefficient of the layers of VEM is directly related to the dimensions of the layer and the shear modulus. This could be verified by a set of new tests and then be compared to the measured damping coefficient from the test set-up.

However, factors such as frictional damping cannot be verified easily. On the other hand, it has been proven with the current test set-up that a rigid connection provides the structural system with a lot more damping than a hinged connection. The exact amount can be studied further in future research.

A modal analysis has been conducted to characterize the frequency dependent behavior of the damping component. However, in the current data analysis the frequency and temperature dependent behavior of the damping component has not been taken into account because in the modal analysis the response was disturbed by other frequencies. Therefore, the results from the modal analysis were not reliable. In future research precautions must be taken in order to avoid these disturbances. For example, the force introduced to the structural system could be filtered by additional layers of rubber. In the current set-up only a small layer of rubber has been used to filter the higher frequencies from the system. By making use of an additional filter and a smaller step size in the frequency domain must lead to a more reliable FRF.

Since only one structure has been analyzed, only one fundamental eigenfrequency was used for the conduction of the tests for this thesis. By adjusting the beam-column connection of the portal frame structure the fundamental frequency was slightly shifted to a lower value. However, for an adequate description of the frequency dependent behavior of the rubber, more tests should be conducted with structures with other eigenfrequencies.

One option could be to change the mass of the structure several times by the use of the same test set-up to shift the eigenfrequencies of the structure to lower and higher frequencies. Then, the corresponding damping ratios can be used to find a curve for the frequency dependent damping ratio.

Preferably, a test set-up with a fundamental frequency of below 1 Hz is needed to properly estimate the behavior of the rubber in a high rise structure subjected to wind load. The fundamental frequency in current measurements was about 2.5 Hz and thus no information is available on damping in the lowest frequency range. For instance, the aspect ratio of 6 could be increased tremendously to decrease the fundamental frequency of the structure by positioning the columns closer to each other.

The test set up was designed to simulate the behavior of a high rise structure subjected to dynamic wind load to the best ability, for instance by using a frame with an aspect ratio of approximately 6. However, it was not possible to lower the eigenfrequency to the desired fundamental frequency with this type of structure. The fundamental frequency was lowered by adding mass to the top of the structure. Nevertheless, adding mass becomes less effective after a certain value. Moreover, from a practical point of view the added mass is limited to the maximum allowed buckling force of the columns of the frame. Another option would be to only study the damper or VEM itself. For instance, the material could be subjected to a hydraulic cylinder which can be tuned beforehand.

Beforehand, the stiffness of the frame has been calculated for two situations:

- 1. A rigid connection of the frame to the floor plate
- 2. The frame connected by simple supports to the floor plate

The fundamental frequency  $f_0$  has been calculated from the corresponding stiffness and effective mass  $m_{eff}$ . The effective mass has been estimated to be 90kg through:

$$m_{eff} = m_{lead} + 0.5 * m_{frame} = 80 + 0.5 * (2 * 1.85 * 3.72 + 6.236) = 90 \text{kg}$$
 (5.1)

Hence, the effective mass consists mainly of the added mass on top of the structure. The effective mass of the frame of  $0.5*m_{frame}$  is an estimation. However, the effective mass from the frame is rather small compared to the mass from the lead blocks on top of the structure. Therefore, it is expected the effective mass has been estimated quite accurately. Nevertheless, in future research, the effective mass can be calculated by calculating the effective mass of the frame from the mode shape of the structure, see also the literature review.

Beforehand, the fundamental frequency was expected to be:

$$1.88 \text{Hz} \le f_0 \le 3.43 \text{Hz}$$
 (5.2)

The measured eigenfrequency was 2.48Hz, which indeed meets the above expectation. Hence, the connection of the frame to the ground was not rigid nor simply supported. This is caused by the welds, which were designed to form a rigid connection but in practice, this has not been the case.

5.1. CONCLUSIONS 55

## 5.1.2 Conclusions of the investigation on the N-MSD system

In this thesis, two methods have been presented to describe the structural system of the high rise structure:

- 1. As a system constructed from mass, springs and dampers
- 2. As a continuous system

The former case is more easy to solve mathematically while the other allows for a detailed description of additional springs and dashpot systems. For example, in case auxiliary damping is introduced in the bracing of the portal frame structure the structural system becomes more complicated. This has been presented in Chapter 4. The bracing can be modeled as a combined spring and dashpot system by the introduction of a matrix system.

Currently, the damping component is modeled as a combination of springs and dashpots as well and each element in the component is studied individually. However, the system becomes rather complicated and thus it is desirable to simplify the system by basic assumptions. These could be made by future research, which should lead to a list of factors to neglect in the model. Additionally, in a high rise structure it is not desirable to implement a damper in series with a stiffness element. Therefore, another damping component or position could be considered in order to obtain a parallel system of the stiffness and damping elements.

In this research, a model has been presented for the core structure with structural damping. The model has been validated in two ways. The stiffness matrix was validated by finding the static behavior of the structure in Section 4.1.1 and the eigenmodes from the structure (Section 4.2.2). Additionally, the peak values for the accelerations come close to the maximum allowed values mentioned in NEN-EN 1990+A1+A1/C2-2011. [30]

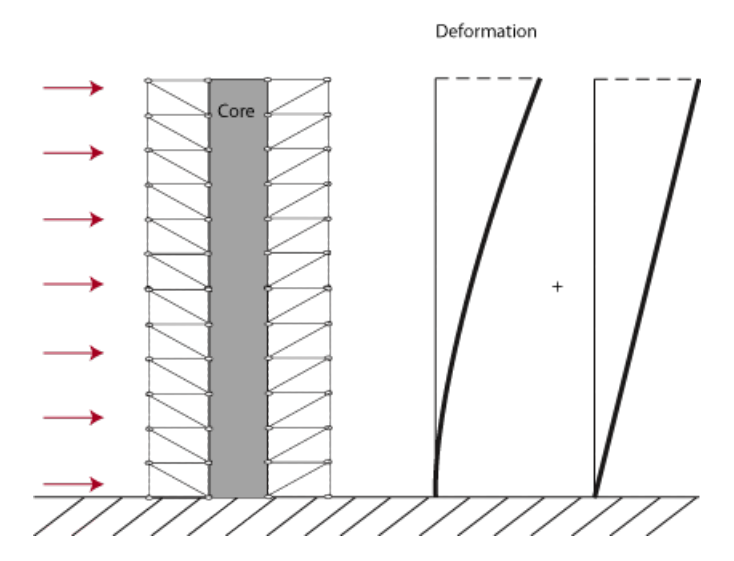


Figure 5.1: A combined core and portal frame structure

Also, the set-up for a braced portal frame structure including an auxiliary damping component has been presented. Since core structures and portal frame structures are often combined in practice, it would be interesting to find a model of the combined structure. In that case, the models presented in this thesis can be used as starting points to define the model of the combined structure. The combined structure (Figure 5.1) requires more detailed information on the structure, for example: by what connections are the two structures connected?

## 5.1.3 Conclusions regarding the prototype tool

The main objective for this thesis has been:

A feasibility study on the development of a prototype tool for engineering firms which can be used to determine the required amount of viscoelastic damping in a high rise structure to reduce accelerations to a comfortable level'

The description of the core structure model and of the portal frame structure prove that it is indeed feasible to develop a prototype tool to determine the required amount of VED. However, more research should be conducted on VED because the behavior of the material remains rather complex. From the literature review it was expected the damping coefficient of the VEM layers could be estimated quite accurately. However, it was not possible to exactly determine the damping coefficient of the layers of VED from the experiment, as was described in Chapter 3. This was due to the fact that the damper was not just in parallel with the spring stiffness of the structure but in series. Additionally, other factors within the damping component could have affected the total damping by the damping component such as frictional forces and the glue layer.

In case a prototype tool is to be developed, input of experimental data of the damping coefficient of the VEM layer is required. This is disadvantageous because experiments are expensive and time consuming. On the other hand, the VEM and its application to the load bearing structure are cheap. Hence, it is expected the total costs of VEDs outweigh the costs of the application of VDs and FDs. This was also the case for the Colombia Center Building, where VEDs only were 1.5% of the total building costs, which even included an extensive testing program. Also, the manufacturer, research institute or engineering firm could once invest in a test set up to investigate different VEMs with different dimensions. The results of these tests could be used in multiple projects and thus it is expected the application of VEMs will become more low-cost over time. [32]

Several test set ups can be considered in order to find the damping coefficient of a VEM. One option, as was conducted in this thesis, is to implement the VEM into a structure and measure the response of the structure. However, a better test set up is a set up with an analysis of the VED. For example, the VEM could be subjected to a load while the displacement could be measured at the same time. The result is a hysteresis loop, which shows the energy dissipation of the VED. In its turn, the hysteresis loop can be used to determine the dynamical material properties of the VEM.

The physical test set-up from this thesis showed that the damping coefficient was influenced by many factors. Therefore, it is advisable to consider a damper including VEM as a whole rather than to analyze the VEM on its own and simply implement some layers of VEM into the structure. In the latter case, the influence of all factors such as the connection of the VEM to the structure must be studied. This is not recommended because executional factors play a large role and thus the effect of the damper can never be really estimated.

The above leads to the following conclusion:

It is feasible to develop a prototype tool to determine the required amount of viscoelastic damping in a high rise structure to reduce accelerations from wind-induced vibrations. Models have been presented for a core and braced portal frame structure including an auxiliary damping component. For the development of the tool the following is recommended:

1. Simplify the model of the bracing including the damping component by making

assumptions from more tests

- 2. The behavior of VEM in a structure must be studied into more detail taking into account the frequency dependent behavior, the dimensions of the layer of VEM and the set-up of the damping component the VEM is being part of
- 3. The model of the single portal frame structure must be extended to a model with N frames stacked on top of one another
- 4. The core and portal frame structure should be combined to a single model to determine the combined behavior by the implementation of VEDs

## 5.2 Extrapolation of the results

In this section, expectations will be presented on how the obtained results will be applicable to other types of high rise structures, other possible positions of VEDs in the load bearing structure, low frequency behavior and damping of the torsional motion through VED.

## 5.2.1 Other positions for VEDs

In the experiment, the layers of SBR were positioned in the bracing in because it was designed to work as a parallel system with the beam. Nevertheless, the beam itself can be adjusted to a parallel spring-damper system as well. Two examples are displayed in Figure 5.2. Both connections are constructed from a gaff connection; the first gaff is connected to the lower flange of the beam and the second gaff is connected to the web of the beam.

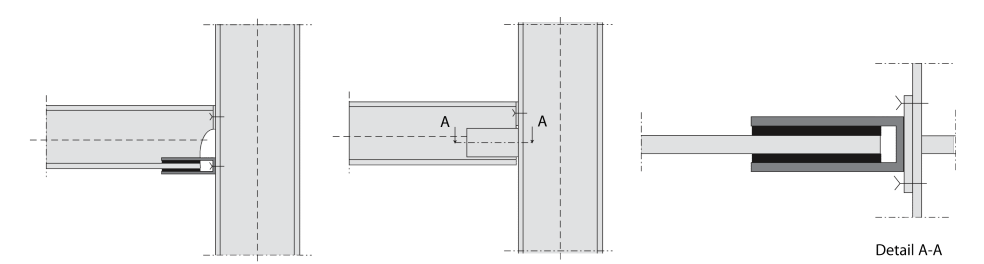


Figure 5.2: Viscoelastic material in beam-column connection

The difference with a damper positioned in the bracing is the effectiveness of the damping. Consequently, the damping coefficient in the bracing  $c_d$  will be increased by  $\frac{b^2}{b^2+h^2}$  in case the damper is positioned in the bracing. Hence, considerations should be made with respect to executional aspects as well as the required amount of damping to determine what position of a damper is best in a certain structure.

## 5.2.2 Damping of torsional motion

In Chapter 2 the importance for reducing torsional accelerations was explained. In case damping in the alongwind direction is considered, the damper is positioned parallel to that direction in order to deform by the force applied to the damper. Therefore, it is expected a damper for the torsional motion will be most effective in case the VEM is positioned in a way it is subjected to torsional motions as well, see Figure 5.3 (left). This principle is already applied in mechanical

engineering for machinery, where torsional vibrations are no exception due to the many rotating elements.

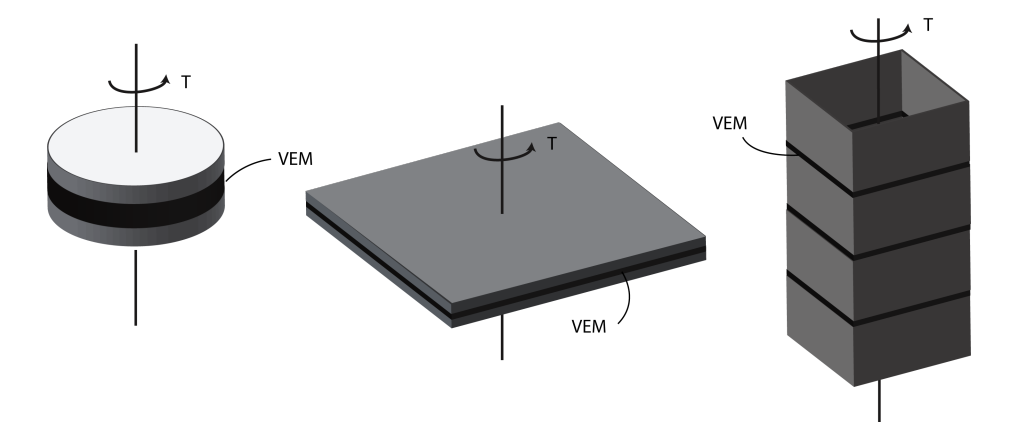


Figure 5.3: Viscoelastic material as a damper for torsional motion

However, in buildings it is more difficult to add a layer of VEM to reduce the torsional motion because the layer could jeopardize the stiffness of the structure. One option for adding layers of VEM to the structure is by an application to the central core of the high rise structure, see Figure 5.3 (right). This same principle could be used for columns in the structure but is expected this will be less effective. Another option could be to add VEM to the connection of the core structure to the rest of the structure for instance, by integrate the VEM to the connection of the core with floors of the building. It is interesting to think of a solution to somehow add VED to the floor of building, see Figure 5.3 (middle) because this principle could be used on multiple positions in the buildings. For example, the floors around rotating columns could be used as well to dampen the torsional motion.

In all solutions mentioned above, the stiffness of the load bearing structure could tremendously decrease by the application of the VEM and thus have to be examined further. Though, as was already demonstrated for the alongwind situation, in case thin layers of VEM are used, the stiffness of the structure is hardly influenced:

$$T = \frac{GJ_T}{t} \qquad \theta \tag{5.3}$$

Especially if the solution with VEM in floors is adopted, the reduction of stiffness by the VEM is expected to be negligible due to the large surface area of the floor.

In literature no solutions were found for dampening the torsional motion with VEDs in buildings and thus the solutions above are only first ideas which could be used as start ups for more ideas. Additionally, in this thesis no attention was paid to the behavior of VEM subjected to a torsional motion. However, it is expected literature will be available on this matter because VEM is often applied in mechanical engineering.

#### 5.3 Recommendations

In this section, recommendations will be made for future research on viscoelastic damping and other factors in a structure that possibly influence the damping

## 5.3.1 Viscoelastic damping

In this section the recommendations with regards to viscoelastic damping will be presented.

## Temperature dependent behavior of SBR

The focus in this thesis has been on the frequency dependent damping behavior of SBR3 and SBR5. It is expected from Figure 3.2 the temperature dependent behavior is stable for SBR used in a building. However, it has not been investigated how the frequency and temperature together influence the behavior of the material. According to Jones (2001), the two factors indeed could be taken into account together by means of a reduced frequency. The reduced frequency is a single variable which takes into account both effects. Hence, this variable and its influence on the damping behavior of SBR could be investigated in future research. Also, tests on this matter could be conducted for other VEMs as well. [17]

## Damping due to extensional deformation

In all calculations and measurements taken from the experiments, the extensional deformation is neglected. It was expected damping through shear deformation was the most effective. However, in some literature a formula for the damping ratio is presented as function of shear and extensional deformation. Hence, it could be reasonable to investigate how the damping behavior of a VEM is effected by extensional deformation. Though, it is still expected damping caused by shear deformation is still the most effective one due to the factors discussed at the start of this chapter.

## 5.3.2 Additional factors that influence the global damping

In Chapter 3 it was clarified executional aspects highly influence the damping behavior of the structure. All single aspects could be investigated further in order to find results applicable to damping in high rise structures.

### Connections

The tighter the connections in the structure, the higher the damping ratio. This was tested for a beam-column connection as well as a bracing-column connection. This observation could be used to find an optimum in high rise structure for the tightness of the connection versus the damping of the structure. The optimum could be found for example by conducting tests on a single connection in which the tightness of the bolt(s) is set as a variable. Also, different types of bolts can be considered as well as different connections.

## Local vibrational mode in perpendicular direction

The application of a stiffer aluminum strip adds more damping to the structure as well. Before the strip was stiffened, the bracing was undergoing local vibrations in the perpendicular direction.

### Connection of viscoelastic material to steel

The layers of SBR were glued to the steel and aluminum parts by 'Vilton Bouwlijm'. All rubber included elements collapsed at some point during the day of testing. Each collapse shows the same failure mode, see Figure 5.4. The glue got loose from the layer of SBR but remained fixed to the steel and aluminum side of the connection. The layer of SBR did not contain any remainders of the glue.



Figure 5.4: Failure mode of the beam

The failure mode raises some question with regards to the connection: is this failure mode caused by a lack of adhesion between the glue and layer of SBR? All parts were thoroughly polished and cleaned before the glue was attached to it, see Appendix C. Is the glue suitable for this purpose? Is the surface of the layer of SBR too smooth? These questions could be answered through a new research on the connection of SBR and other VEMs to steel. However, in case many dampers are to be applied in a building, it is more convenient to invest in the vulcanization of VEM to steel.

# 6 Summary of conclusions

This chapter provides the reader with a summary of the conclusions and recommendations from Chapter 5.

#### Conclusions regarding the investigation on VED:

- The damping ratio can be determined in the frequency domain by the half-power bandwidth method and from the time signal through the logarithmic decrement. Both methods can be used to verify the result obtained from the other method
- The global damping of the structure can be increased by many factors:
  - Damping by friction
  - Material damping
  - Factors within the damping component:
    - \* Damping by friction
    - \* Material damping
    - \* Damping by adhesive layer (glue)
    - \* Layers of viscoelastic material

If a higher damping coefficient is required to reduce accelerations, each of these factors may be changed.

- The exact energy dissipation by each individual factor remains still unkown. The only certainty is that the component as a whole dissipates energy from the structural system and reduces the accelerations.
- It has been proven with the current test set-up that a rigid connection provides the structural system with a lot more damping than a hinged connection. The exact influence can be studied further in future research.
- To avoid disturbances in the signals by higher frequencies, a filter such as a rubber layer may be used to introduce the force to the system
- The frequency dependent behavior of the SBR layers should be studied further for example by changing the mass of the structure several times by the use of the same test set-up to shift the eigenfrequencies of the structure to lower and higher frequencies.
- To study the low-frequency range behavior of the VEM, a structure has to be designed with a fundamental frequency of below 1Hz. For instance, the aspect ratio of 6 could be increased tremendously to decrease the fundamental frequency of the structure by positioning the columns closer to each other.

- The influence of the mass of the frame becomes rather small by the application of added mass to the structure. However, the effective mass of the frame could be calculated precisely from the corresponding mode shape of the structure
- The measured fundamental frequency may be compared to the calculated fundamental frequency in order to determine the type of connection of the frame to the floor plate

### Conclusions of the investigation on the N-MSD system

- Structures can be modeled through two methods:
  - 1. As a system constructed from mass, springs and dampers
  - 2. As a continuous system
- Introduction of a damping component in the bracing leaves a combined spring and dashpot model for the bracing, both in series and parallel.
- In a high rise structure it is not desirable to implement a damper in series with a stiffness element. Therefore, another damping component or position could be considered in order to obtain a parallel system of the stiffness and damping elements.
- In practice, core and portal frame structures are often combined to one structure and thus it is convenient to find an equivalent model for that in future research

#### Conclusion regarding the prototype tool:

- The description of the core structure model and of the portal frame structure prove that it is indeed feasible to develop a prototype tool to determine the required amount of VED.
- In case a prototype tool is to be developed, input of experimental data of the damping coefficient of the VEM layer is required. Two methods are suggested:
  - 1. Implement the VEM into a structure and measure the response of the structure (as was presented in this thesis)
  - 2. Analysis of the VED only by subjecting the damper to a load while the displacement could be measured at the same time. The result is a hysteresis loop, which shows the energy dissipation of the VED.
- It is feasible to develop a prototype tool to determine the required amount of viscoelastic damping in a high rise structure to reduce accelerations from wind-induced vibrations. Models have been presented for a core and braced portal frame structure including an auxiliary damping component. For the development of the tool the following is recommended:
  - 1. Simplify the model of the bracing including the damping component by making assumptions from more tests
  - 2. The behavior of VEM in a structure must be studied into more detail taking into account the frequency dependent behavior, the dimensions of the layer of VEM and the set-up of the damping component the VEM is being part of
  - 3. The model of the single portal frame structure must be extended to a model with N frames stacked on top of one another
  - 4. The core and portal frame structure should be combined to a single model to determine the combined behavior by the implementation of VEDs

#### Recommendations for future research:

- More tests have to be conducted to properly analyze the frequency dependent behavior of SBR
- The influence of the temperature and frequency on SBR together could be analyzed further although the temperature in a building is stable
- The damping by extensional deformation has not been studied in this thesis
- The tests showed that the connections in a structure highly influence the damping of the structure. This could be a starting point of a research on this aspect
- The connection of SBR to the steel and aluminum parts collapsed. Future research could clarify what connection is best to use
- The influence of the low frequency range to the damping behavior of VEM could be analyzed further because this is important for dampening wind-induced vibrations
- The N-MSD model could be developed further
- Damping of the torsional motion by VED could be investigated
- The non-linear region of VEM could be studied since the loss factor in this region is higher and thus the VED will be more effective than for low values of the loss factor

# **Bibliography**

- [1] Ali M.M., Moon K.S., 2007, Structural Developments in Tall Buildings: Current Trends and Future Prospects, university of Sydney
- [2] Aquino R.E.R., Tamura Y., 2013, On stickslip phenomenon as primary mechanism behind structural damping in wind-resistant design applications, Journal of Wind Engineering and Industrial Aerodynamics vol.115 p.121-136
- [3] Berg R.L.J. van den, 2012 Investigation of damping in high-rise building, TU Delft
- [4] Bilbao A., Avils R., Agirrebeita J., Ajuria G., 2005, *Proportional damping approximation for structures with added viscoelastic dampers*, Finite elements in analysis and design 42
- [5] Blaauwendraad prof. dr. ir. J., 2005, Dynamica van systemen, TU Delft, page 43-44
- [6] Blaauwendraad prof. dr. ir. J., 2006, Plate analysis, theory and application, volume 2 numerical methods, TU Delft
- [7] Breen H., 2007, Tall storeys: active control of wind impact on high-rise buildings, TU Delft
- [8] Callister W.D.Jr, 2003, Materials science and engineering An introduction, John Wiley and Sons
- [9] Cook N.J., 1985 The designers guide to wind loading of building structures, The University Press Cambridge
- [10] eFluids.com, http://www.princeton.edu/ asmits/Bicycle web/Bernoulli.html(Accessed at february 21nd 2013), Princeton University
- [11] http://www.emporis.com/statistics/worlds-tallest-buildings (checked at november 29 2012)
- [12] Hoenderkamp J.C.D., 2007, High-rise structures, preliminary design for lateral load, Eindhoven University of Technology, chapter 2 and 3
- [13] Holmes J.D., 2001, Wind loading of structures, Taylor & Francis
- [14] Hoorn H., year unknown, Vergrotingsfactoren Zalmhaven DO fase aangepast, Zonneveld Ingenieurs
- [15] Horr A.M., Schmidt L.C., 1996, Modelling of nonlinear damping characteristics of a viscoelastic structural damper, Engineering Structures vol.18 no.2 pp.154-161
- [16] Jeary A.P, 1981, The dynamic behaviour of tall buildings, University College London

BIBLIOGRAPHY 65

[17] Jones D.I.G., 2001, Handbook of viscoelastic vibration damping, John Wiley & Sons Ltd.

- [18] Kareem A., Kijewski T., Tamura Y., 1999, Mitigations of motions of tall buildings with specific examples of recent applications, Wind and structures vol. 2 no. 3, page 201-239
- [19] Kuroda H., Arima F., Baba K., Inoue Y., 2000, Principles and characteristics of viscous damping devices (gyro-damper), the damping forces which are highly amplified by converting the axial movement to rotary one, 12th world conference on earthquake engineering
- [20] Lai M.L., Lu P., Lunsford., Kasai K., Chang K.C., 1996, Viscoelastic damper: a damper with linear or nonlinear material?, Elsevier Science Ltd.
- [21] Li Q.S., Yang K., Zhang N., Wong C.K., Jeary A.P., 2002, Field measurements of amplitude-dependent damping ga 79-storey tall building and its effect on the structural dynamic responses, Structural design tall buildings no. 11, Whiley InterScience
- [22] Löhnert G., Dalkowski A., Sutter W., 2003, Integrated design process A guideline for sustainable and solar-optimised building design, International Energy Agency
- [23] Lu L., Chung L., Wu L., Li G., 2004, Dynamic analysis of structures with friction devices using discrete-time state-space formulation, Computers and structures, page 1049-1052
- [24] Lythe G.R., Surry D., 1990 Wind-Induced Torsional Loads on Tall Buildings, Journal of Wind Engineering and Industrial Areodynamics, no. 36, page 225-234
- [25] Marui E., Endo H., Hashimoto M., Kato S., 1996, Some considerations of slideway friction characteristics by observing stick-slip vibration, Tribology International vol. 29 no. 3 pp. 251-262, Elsevier Science ltd
- [26] Metrikine A.V., year unknown, Slender Structures and Introduction to Continuum mechanics; Module: Dynamics of Mechanical Systems and Slender Structures: Lecture Notes CT 4145, TU Delft
- [27] NASA, year unknown, URL: http://www.grc.nasa.gov/WWW/BGH (Accessed at february 25th 2013), NASA
- [28] Nemetschek Scia nv, 2011, Advanced Professional Training Dynamics, Scia Engineer
- [29] NEN, 2011, National Annex to NEN-EN 1991-1-4+A1+C2: Eurocode 1: Actions on structures Part 1-4: General actions Wind actions, Nederlands Normalisatie-instituut
- [30] NEN, 2011, National Annex to NEN-EN 1990+A1+A1/C2-2011: Eurocode 1: Basis of structural design, Nederlands Normalisatie-instituut
- [31] Nijsse prof. R., 2012, Lecture slides Buildings Structures II (guest lecture), Delft University of technology
- [32] Oosterhout G.P.C. van, 1996, Wind-induced dynamic behaviour of tall buildings, TU Delft

66 BIBLIOGRAPHY

[33] Pasquin C., Leboeuf N., Pall R.T., Pall A., 2004, Friction dampers for seismic rehabilitation of Faton's building, Montreal, 13th world conference on earthquake engineering, page 1-2

- [34] Robbemont A.J., 1995, The dynamic behaviour of tall buildings as a design criterion, TU Delft
- [35] Simone A., 2011, An Introduction to the Analysis of Slender Structures, TU Delft, ch. 2-3
- [36] Skyscraper Group, 2011, URL: www.skyscraper.com (Accessed at december 15 2012), Skyscraper group
- [37] Smith B.S, Coull A., 1991, Tall Building Structures Analysis and Design, John Wiley & Sons Inc., page 1
- [38] Smith R.J., Willford M.R., 2007, The damped outrigger concept for tall buildings, John Wiley & Sons
- [39] Spijkers J.M.J, Vrouwenvelder A.W.C.M., Klaver E.C., 2005, Dynamics of structures part 1 vibration of structures, TU Delft
- [40] Steenbergen R.D.J.M., 2007, Super Elements in High-Rise Buildings under Stochastic Wind Load, TU Delft
- [41] TA Instruments, 1998, Energy storage and dissipation in viscoelastic materials, TA Instruments
- [42] Thorne K, year unknown, *URL: http://www.pma.caltech.edu/Courses/ph136/yr* 2004/book03/chap05/0205.1.pdf (Accessed at december 2nd 2012), California Institute of Technology
- [43] Vrouwenvelder A.W.C.N, 2004, Random vibrations, TU Delft
- [44] Vuik C., Beek P. van, Vermolen F., Kan J. van, 2006, Numerieke methoden voor differentiaalvergelijkingen, VSSD, chapter 6
- [45] Wang J., Jin F., Zhang C., 2011, Estimation error of the half-power bandwidth method in identifying damping for multi-DOF systems, Tsinghua University, Beijing
- [46] Yu C., Roesset J.M., 2001, Dynamic stiffness matrices for linear members with distributed mass, Tamkang Journal of Science and Engineering, Vol. 4, No. 4, pp. 253-264
- [47] Zegers S.F.A.J.G., 2011, Lightweight floor system for vibration comfort, Eindhoven University Press Facilities

